An In-Fiber Michelson Interferometer Long-Period Grating (LPG)

With

Integrated Sol-Gel and Aptamer Coatings for Biosensor Development.

By

YAO XIAO B.Sc

A Thesis

Submitted to the School of Graduate Studies

in Partial Fulfilment of the Requirements

for the Degree

Master of Applied Science

McMaster University

© Copyright by Yao Xiao, August 2010

MASTER OF APPLIED SCIENCE (2010)   McMaster University

(Engineering Physics)   Hamilton, Ontario

TITLE: An In-Fiber Michelson Interferometer Long-Period Grating (LPG) With

Integrated Sol-Gel and Aptamer Coatings for Biosensor Development.

AUTHOR: Yao Xiao, B. Sc. (Huazhong University of Science and Technology)

SUPERVISOR: Professor Chang-Qing Xu

Professor John Brennan

NUMBER OF PAGES: IX, 97

Abstract

In this work, an in-fiber Michelson interferometer Long-Period Grating (LPG) biosensor with integrated sol-gel and aptamer coatingd was used for the development of a biosensor for adenosine triphosphate. A macroporous gold-nanoparticle doped sol-gel derived silica film was coated on the sensing head to enhance surface area and the sensitivity of the LPG based biosensor and to act as a surface for subsequent aptamer immobilization. The large surface area of the sol-gel film increases the number of immobilized aptamers, while the presence of the gold nanoparticles improves the refractive index match with the fiber cladding, enhancing sensitivity. The thin film, which is only two hundred nanometers thick, ensures the evanescent wave penetrates into the ambient environment. The LPG sensor has been demonstrated to work for the selective sensing of ATP in solution. The origin of the sensitivity enhancement is confirmed via simulation and experiments which included the design and fabrication of the LPG sensor.

Acknowledgement

I would like to thank Dr. Chang-Qing Xu and Dr. John D. Brennan for their guidance and support in the past two years. Without their guidance and help, it is impossible to finish the research work and this thesis. Thanks to my committee members Dr. Chang-Qing Xu, Dr. John Brennan, and Dr. Qiyin Fang for taking the time reading my thesis and attending my defense meeting. This ensures a high quality of the defense meeting and the degree. I also want to thank Dr. Yingfu Li, who taught me a great deal about aptamers.

Strong support from other members in Dr. Xu's and Dr. Brennan's labs is indispensable in completing this work. They taught me new techniques and knowledge, showed me how to solve problems, overcome difficulties and discover new things. Dr. Wangguo Liang, Dr. Yang Lu, Dr. Zakir Hossain, Dr. Hanjiang Dong, Ms. Carmen Carrasquilla, Mr. Qingyang Xu, Mr. Yi Gan, Mr. Jian Sun, Mr. Nikolas Eleftheriou, Ms. Meghan McFadden, Ms. Erica Forsberg and Ms. Anne Marie Smith gave me so much help during the whole process of research. Other important help was from Dr. Jian Yang and Pawan Sandhu, who are the previous students working on this project. Without your help, it would be very hard for me to start an unfamiliar new project all by myself.

Contents

List of Figures

List of Tables

Chapter 1 Introduction

1. Sensors

A sensor is a device that measures a physical quantity and converts it into a signal which can be read by an observer or by an instrument [1]. This physical quantity is usually beyond human measuring capabilities. Sometimes the value is too low and sometimes it is dangerous and not suitable for a human-being to measure the quantities. Sensors are used in everyday objects with innumerable applications such as cars, machines, aerospace, medicine, manufacturing, robotics and biochemistry.

1.1 General Description of a Biosensor

In the world, pathogenic bacterial infections cause severe illnesses and death every year. Thus, there is a need to develop detection methods that are both rapid and sensitive. The conception of the biosensor was brought in by Clark in the 1960s [2]. Since that time, biosensors have attracted significant interest as they have many applications in the biological and medical area, especially in in bio-molecule detection. Biosensor development is driven by the continuous need for simple, rapid, and continuous in-situ monitoring techniques in a broad range of areas, e.g. medical, pharmaceutical, environmental, defense, bioprocessing, or food technology.

A biosensor is a device for the detection of an analyte that combines a biological component with a physicochemical detector component. It usually consists

of 3 parts: The first part is the sensitive biological element. The biological element can be natural o r fabricated via biomedical or biological engineering. It is usually a biologically derived material, biomimic or biologic material such as tissue, microorganisms, organelles, cell receptors, enzymes, antibodies, nucleic acids and so on. The second part is the transducer or detector element which is used to transform the signal that results from the interaction between the analyte or target with the biorecognition element into another signal which is much easier to measure and quantify than the original one. There are several ways to implement this, such as physicochemical, optical, piezoelectric and electrochemical methods. The third part is the associated electronics or signal processor that is primarily responsible for the processing and display of the results in a user-friendly manner. The greatest difference between optical biosensors and other biosensors is in the transducer which usually uses components such as photodetectors, charge-coupled device (CCD) arrays and fibers to transfer the biological signal to an optical signal [3]. Figure 1.1 shows the general structure of a biosnesor. When a reaction occurs between the biological element and the analyte target, a signal is detected by the detector and converted to an electronic signal through several steps and ultimately displayed via a signal processing equipment.

1.2 Classification of Optical Biosensor.

Optical biosensors can be classified according to many different criteria, such

as by the analyte, by the biological recognition element, by the application or by the

physicochemical transducer. The optical biosensor can be classified into label-based

and label-free biosensor by the immobilization and transduction mechanism [4].
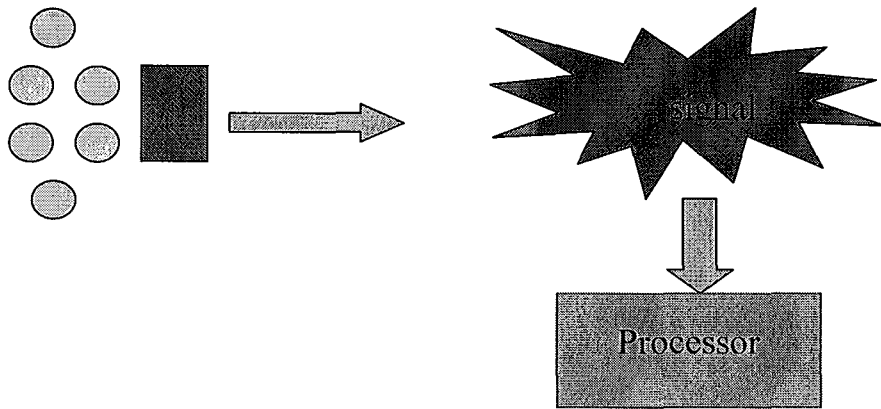
Figure 1.1 General structure of the biosensor

1.3 Label-Based Biosensor

In the label-based biosensor, a chromophore or fluorophore is used to generate

a signal upon analyte binding. The fluorescence technique is most widely used

nowadays as it can provide more sensitive detection of biomolecules. Fluorescent

biosensors can detect low analyte concentrations as the fluorescence signal is

proportional to the excitation intensity, increasing sensitivity when laser sources are

used.

There are several methods to produce or consume the fluorescence species.

For example, NAD^+ (nicotinamide adenine dinucleotide)-dependent reactions, which

are catalysed by a group of dehydrogenase enzymes, are some of the

3

enzyme-catalysed reactions which can cause the phenomenon

$$Sbstrate + NAD(P)^+ \xrightarrow{dehydrogenase} product + NAD(P)H$$
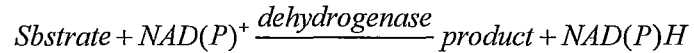
In this reaction, the NADH is produced. It is the fluorescence species. Its excitation

wavelength is 350 nm and emission wavelength is 450 nm which can be collected by a

fiber or detected by a photo-detector. There are also many other examples for the

dehydrogenase or oxidoreductase enzymes producing fluorescent species in optical

fluorescence biosensors.

Fluorescence-based optical biosensors usually combine a bioreceptor with

fluorescence into the sensor which can cause a signal in the optical transducer. The

biosensing layer is usually coated at the end of the optical fiber, which can generate

fluorescent signal and detected by the fiber. In this process, the optical fiber

propagates the excitation light to the fluorescent molecules and then propagates the

fluorescent light back to a detector to measure. When the biomolecules are

immobilized, the sensor should be shielded from extraneous light, which can make the

fluorescent signal collection easier and avoid the interference from background noise.

However, sometimes, in order to simplify and enhance the reliability of the biosensor,

the sensor should be configured to allow operation in an ambient light.

There is one type of fluorescent optical biosensor reported by Anderson [5]

(Figure 1.2). It uses an optical fiber to integrate the optical and electrical part of the

sensor together and then detect the analyte. First, the end of the fiber is etched and tapered and then coated with antibodies or protein. The fiber is immersed into solution containing a fluorescently labeled ligand molecule. After a few seconds, the interaction occurs between the bio-receptor on the fiber and the target molecule in the solution which lead that a few fluorescent tagged biomolecules transferred onto the fiber and can be detected by a photomultiplier tuber (PMT) or photodiode.
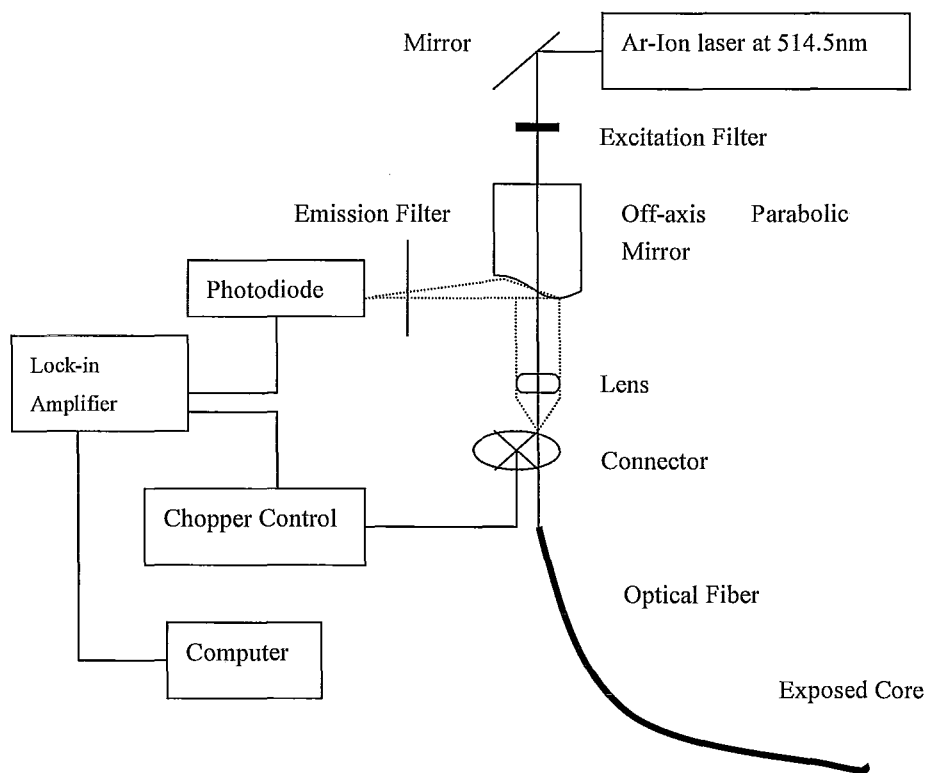
Figure 1.2 Structure of the fluorescent optical biosensor [5]

There are many other applications of the labeled biosensors in the medical sciences, environment protection and pollution processing. This is also widely used in

the DNA sequencing [6] and visual tracking and imaging of biomolecules [7]. The label-based biosensor uses the fluorescence signal which is proportional to the biosensing signal, so it can be detected even though it is weak. Then many properties of the fluorescent light can be detected and a multiple signal can be generated. However, when it refers to the immunoassay, it is not as good as expected. The fluorescent molecules which attached on the bio-receptor or target molecules will have some chemical reaction and interfere or hinder the process, so labeled biosensors are not ideal in this case. Thus label-free biosensors have been introduced, which don't need tagged biomolecules to achieve detection. The fluorescent biosensor also has photobleach and background light interference. Moreover, the label-free biosensors are more portable and can give us a new angle to enhance the sensitivity.

1.4 Label Free Biosensors

The label-free biosensor doesn't require any additional biomolecules to be attached on the bio-receptor or target to generate a signal, and the binding process isn't influenced by the extra biomolecules. In the label-free optical biosensor, the optical properties of the bioreceptor always have some changes when the target molecule interacts with the bio-recognition film. The optical properties before and after the interaction are recorded and compared and then the signal, which is based the changes of the optical properties, is obtained. Usually, the optical property used is the index of refraction as it usually reflects the optical density of the medium and has a

direct influence on any light wave propagating in the medium. When the target molecules react with the bio-receptors, the electron field distribution is usually changed and it will result in the change of index of refraction. The sensitivity of the label-free optical biosensor which works in this way is usually defined by how much signal it can induce for a given change in refractive index of the sensing layer.

1.4.1 SPR Biosensor

In the past two decades, surface plasmon resonance (SPR) sensing has proven to be a useful quantitative probe of the interactions of a variety of biomolecules with various ligands, biomolecules, and membranes, including protein:ligand, protein:protein, protein:DNA and protein:membrane binding. It provides a means not only for identifying these interactions and quantifying their equilibrium constants, kinetic constants and underlying energetics, but also for employing them in very sensitive, label-free biochemical assays [8].

In a typical SPR biosensing experiment, a glass slide with a thin gold coating is mounted on a prism.   Light passes through the prism and slide, reflects off the gold and passes back through the prism to a detector. A flow cell allows solutions above the gold surface to be rapidly changed. The bioreceptor in the interactant pair is immobilized on an SPR-active gold-coated glass slide which forms one wall of a thin flow-cell, and the target molecule in an aqueous buffer solution is induced to flow

across this surface, by injecting it through this flow-cell (Fig. 1.3). Changes in reflectivity versus angle or wavelength give a signal that is proportional to the volume of biopolymer bound near the surface. When light (visible or near infrared) is shined through the glass slide and onto the gold surface at angles and wavelengths near the so-called "surface plasmon resonance" condition, the optical reflectivity of the gold changes very sensitively with the presence of biomolecules on the gold surface or in a thin coating on the gold. The high sensitivity of the optical response is due to the fact that it is a very efficient, collective excitation of conduction electrons near the gold surface. The extent of binding between the solution-phase target and the immobilized bio-receptor is easily observed and quantified by monitoring this reflectivity change. An advantage of SPR is its high sensitivity without any fluorescent or other labeling of the interactants [8].
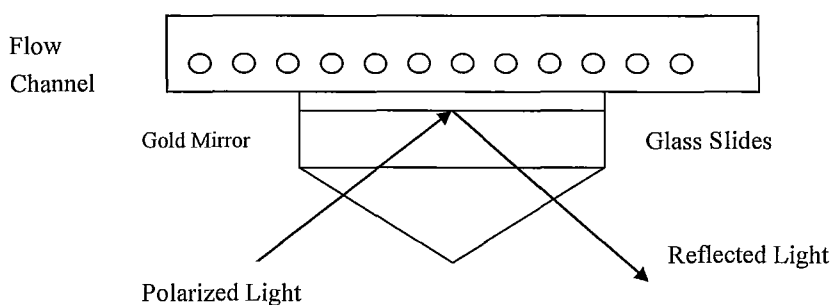
Figure 1.3 Basic components of an instrument for SPR biosensing [8]

Figure 1.4 is another type of SPR biosensor (Spreeta system) fabricated by Texas Instruments. There are some differences between the instrument in Figure 1.3,

(Biacore), and the Spreeta. In the Biacore system, the chips that can be removed are usually fabricated previously with appropriate binding bioreceptors and can be replaced for different applications. It also has a microfluidic system for delivering solution with analyte. However, the Spreeta is more compact and it is more difficult to replace its sensor chips and it also lacks the sealed encasing and solution delivery system.   B iacore is the most popular commercial instruments for SPR biosensing [9]

Such SPR biosensing has found a very wide variety of applications, has contributed data to thousands of scientific publications on biomolecular interactions, and has enjoyed substantial commercial success. However, they are expensive and require critical fabrication procedures. As well, there is a need to compact and miniaturize the designs for more versatile use. In order to do so, researchers have used optical fibers to fabricate novel sensors.
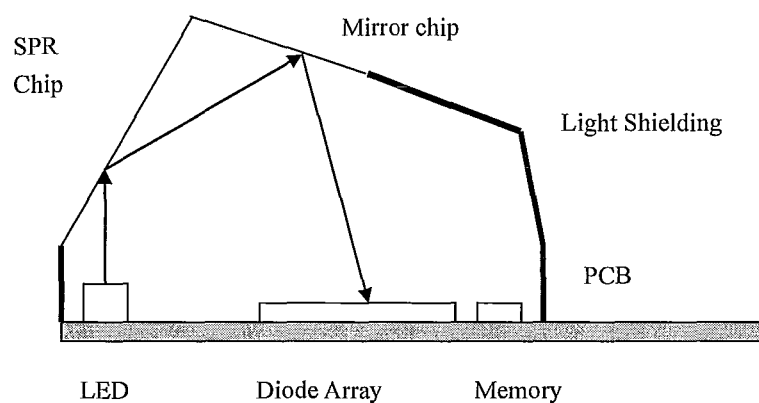
Figure 1.4 Schematic Figure for the Spreeta [9]

1.4.2 Fiber Optic Label-Free Biosensors

Optical Fibers are the mediums for propagating light and mostly used in optical communication systems. Nowadays, fibers are also used in some others applications, especially for sensing. Fiber optic biosensors are biosensors which use the fiber as the transducer element by using the characteristics of light transmission along the fibers. Fiber Optic Biosensor can be implemented within different techniques described below.

1.4.2.1 Absorbance Fiber Optical Biosensor

By absorbing a fixed wavelength of light, fiber optic biosensor can measure any changes in the concentrations of absorbing analytes according to Beer's Law, which is the simplest fiber optical biosensor. The system works in the following principle: The light is transmitted trough the fiber to the testing sample. After that, the absorbance of the light by the sample is detected by the same fiber or another fiber. The bio-recognition film is immobilized at the distant end of the optical fiber and either produces or measures the capability of the analyte for absorbing the light.

Wolthuis et al. reported a fiber optics pH sensor for medical applications (Figure 1.5) [10]. An absorptive indicator compound is used by the sensor. Its wavelength absorbance peak is near 625 nm. Moreover, pH change in the range of 6.8 to 7.8 will cause a linear change in the light absorption. A pulsed red light-emitting

diode (LED) emits light into the sensor. The diachroic mirror can be passed through

by a small range of light while reflects others, so the returning light is split into short

wavelength and long wavelength components by a dichroic mirror. The signals are

detected by photodiodes. Then the photocurrents can be used as a biosensing signal to

be measured and processed. In his report, it said the sensor could provide a resolution

of 0.01 pH and the response time is about 30-40s. Following the gamma sterilization,

the sensor testing with heparinised human blood had an excellent agreement with the

clinical blood gas analyzer. It demonstrated the sensor had a good performance and

low cost.
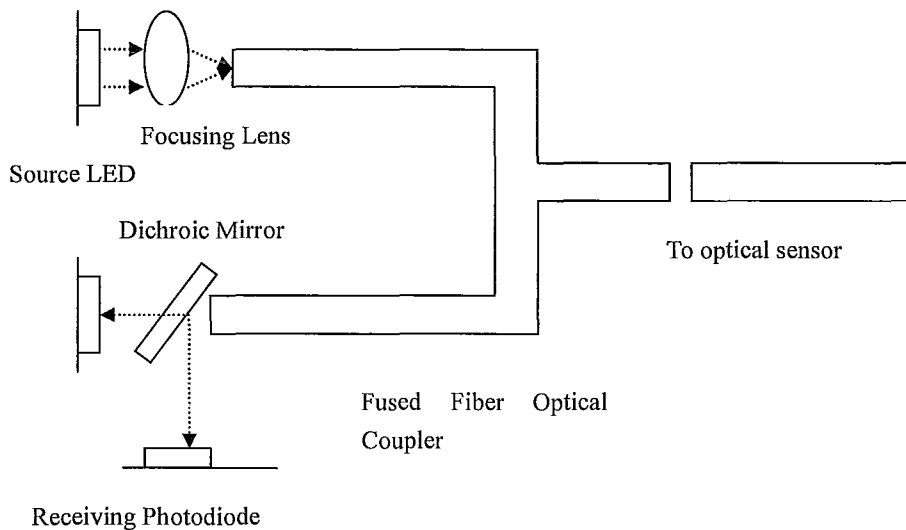
Figure1.5 Structure of the fiber optical pH sensor [10]

In addition, Wolthuis also reported another biosensor and it is a fiber optical

oxygen sensor. In this sensor, the sensor's indicator becomes strongly absorbant after

the UV simulation, and then returns to the transparent state. What he measured is the rate of the indicator return to transparency as it is proportional to the local oxygen concentration. The indicator is also monitored by a red LED. It is reported that this system has comparable performance to the existing oxygen measurement techniques.

1.4.2.2 SPR Optical Fiber Biosensors

There are three types of fiber optical SPR biosensor reported recently. The left structure in figure 1.7 is the simplest one. It is a single mode fiber with a metal coated distant flat end. The light propagates in the core of the single mode fiber, which is usually a standard fiber for the optical communication. The light is reflected by the metal coating and goes through a circulator and input into an optical spectrum analyzer (OSA). In the SPR optical fiber biosensor, the light is usually considered as light beams, not the wave. If you want to excite the surface plasmon wave (SPW) at the metal layer surface, the light should be incident in a specific angle and at a specific wavelength. The interrogation wavelength is limited as the numerical aperture of the fiber only allows a limited range of the incident angles. The wavelengths are near the infrared and below. As the usual communication wavelength is in the mid-infrared wavelength, the SPR optical fiber biosensor is out of this range and thus stricter requirement in the optoelectronic components development and fabrication [12].

However, the operating wavelength is almost fixed, so an improved structure

is reported which is shown in the middle figure of Figure 1.7, which doesn't use the

flat end. It uses a chemically etched conical sensing surface instead, so the cone angles

can be changed if we adjust the etching parameters and it is much more flexible than

the first structure. But in both the first structure and the second structure, the sensing

surface is rather small because the sensing surface is determined by the diameter of

the fiber core. However, the core of a single mode standard fiber is only around or

below 10 um [12].

As there are so many limitations of the first and second fiber optical SPR

sensor structure, a third structure was implemented which is shown in the right figure

of Figure 1.6. In this structure, the cladding of the optical fiber is etched by the

chemicals, so the fiber core is exposed in a certain defined length and coated with a

metal layer and a bio-receptor layer on top of it. The interaction area is greatly

increased. However, another problem appears. The bare fiber core is very fragile and

the mechanical stability of the fiber optical SPR biosensor is greatly decreased. It is

very difficult to handle the sensor as the small fiber core is very easily broken if a

protection layer is not added on to the fiber. Another problem is this type of sensor has

two ports, an input port and an output port which means it works in the transmission

mode, not the reflection mode. As the sensing part is very brittle, it is very difficult to

immerse the sensor into the target molecule solution if the sensor has two ports and

the sensing part is in the middle of the sensor. In this case, it is much more desirable to

make a fiber optical sensor in the reflection mode which only has one port and it is much easier to immerse the sensor into the target molecule solution [12].
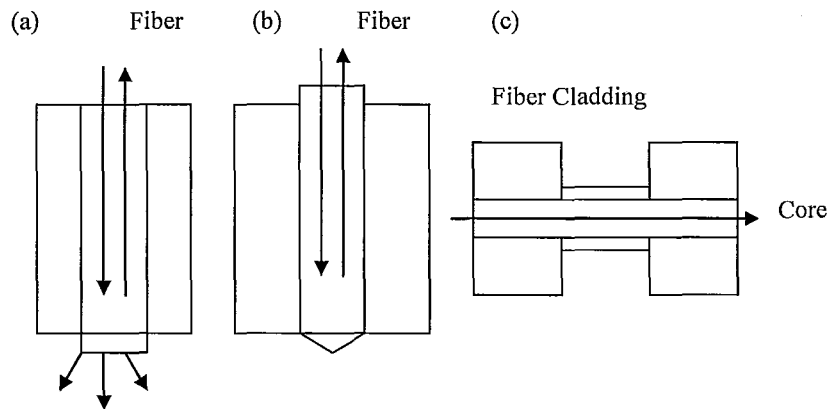
Figure 1.6 Three types of SPR fiber optical biosensor [12]

Of course, the fiber optical SPR biosensor has much more advantages than the bulk SPR optical biosensor because it is more portable and much less expensive in the fabrication as it is fabricated by the fiber which is very cheap and very tiny. However, it also has some disadvantages as it is very fragile and easily broken and it is also less flexible than the bulk SPR optical biosensor.

1.4.2.3 Grating Based Fiber Optical Biosensor

Grating is an optical component with a periodic structure, which is used to split and diffract light into several beams propagating in different directions. The grating spacing and the light wavelength can determine the beam splitting or

diffraction directions.

When the fiber is located in the hydrogen for a certain time, the hydrogen molecules will diffuse into the fiber. It will lead to a dissociation of the hydrogen molecules when the fiber is exposed to the UV radiation. The Si-OH and / or Ge Oh will be formed. Along with this, there is formation of the Ge oxygen deficient centers, leading to a refractive index change. Then the refractive index of the fiber will be modified depending on the strength of the light. This technique is usually used to cause periodical refractive index change and fabricate the fiber grating [13].

There are usually two types of grating-based fiber optical biosensor. The first type is Fiber Bragg Grating (FBG) biosensor, which is also called short period grating (SPG) biosensor. The second type is the long period grating (LPG) biosensor.

An FBG is a type of distributed Bragg reflector constructed in a short piece of optical fiber which can reflect specific wavelengths of light and transmits all the others. This can be implemented by periodical modulation of the refractive index of the fiber core. The period of the FBG is usually short and only several micrometers, so it belongs to the short period grating.
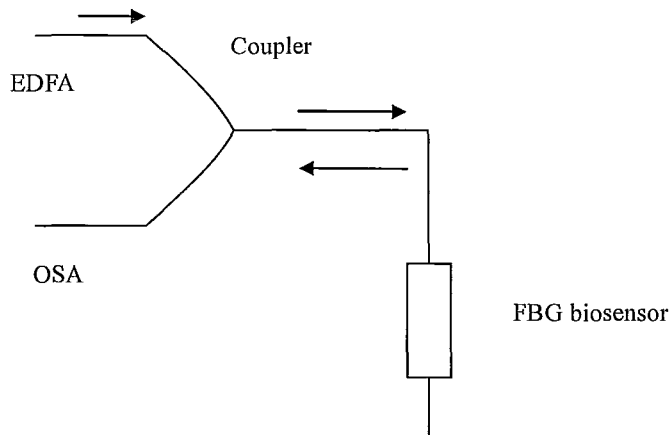
Figure 1.7 Structure of the FBG biosensor [14]

For the fiber grating biosensor which uses the propagation modes, the sensor is sensitive to the ambient refractive index change because there are evanescent wave penetrating into the ambient. In this case, the key issue with the FBG biosensor system is to achieve a strong enough evanescent wave to penetrate into the ambient environment. When it refers to the FBG biosensor, the usual method is to use a chemical to etch the cladding around the FBG and make the ambient environment the cladding, which can greatly enhanced the evanescent wave. A FBG biosensor has been reported that has successfully implemented this strategy (Figure 1.7), using the FBG cladding etching method. In the FBG working principle, the propagation constant of the core mode depends on the cladding refractive index. In this case, the Bragg wavelength will change if the ambient refractive index changes, which can be observed in the optical spectrum analyzer [14].

Long Period Grating (LPG) Biosensor is another type of biosensor. A long period grating is a fiber grating with a relative long period, compared to FBG and other short period grating. Its period is usually in the order of the millimeter. It can couple a guided core mode to the cladding modes which is wavelength dependent.

The LPG is a transmission grating (Figure 1.8). Usually two LPGs are fabricated in the same fiber. The section of the fiber between the two LPGs is the sensing part and usually coated with a bio-recognition film. When light is introduced from one port of the sensor, it usually propagates in the core. After it meets the first LPG, part of the core mode is coupled to the cladding mode and propagates in the cladding. The rest of the core mode will propagate in the core. When the light meets the second LPG, the cladding mode will be coupled back into the core and cause the interference with the core mode. The change of the refractive index of the ambient around the sensing part of the LPG sensor will change the effective index of the cladding mode which is reflected in the interference spectrum [15].

Cladding

Core
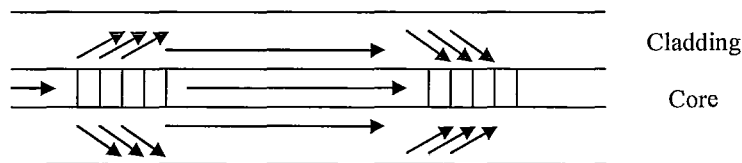
Figure 1.8 Structure of the LPG biosensor [15]

1.5 Sol-gel derived silica material

Sol-gel processing of materials is a technology with a long history. The earliest sol-gel work can be dated to 1846 when it was observed that the hydrolysis of tetraethyl orthosilicate (TEOS) under acidic conditions led to the formation of a layer of SiO_2 in the form of silica fibers or monoliths. Sol-gel work continued to develop in the following one hundred and fifty years and became very important in the 1990s when it showed that the method can be used to immobilize biomolecules within silica. Until now, more than 35,000 papers were published worldwide on this area [16].

Among the techniques for biomolecule immobilization, the sol-gel method is one of the most famous ones, as it is widely used in the material science and biochemistry engineering. In the sol-gel process, the material fabrication is done from a liquid precursor sol-gel. The solution which usually consists of colloidal silica in an aqueous or alcohol solution (the sol) starts to gel and forms the discrete particles or network polymers. The most common precursors are metal alkoxides and metal chlorides. Sodium silicate is also used as the precursor. The sol-gel precursor can usually undergo various forms of hydrolysis and polycondensation reactions as it gets to form a solid product [16].

In the sol-gel process, the sol is usually considered as a solution, but it will gradually change to a diphasic material which means it includes both a solid phase and

a liquid phase. Its morphology is varied and can be easily controlled. Sometimes it is

discrete particles. In other cases, it can form polymer networks. An important step for

the sol-gel process is to remove the extra amount of the liquid part because the particle

density may be too small and it can't be regarded as a colloid. Removable of the extra

liquid is usually done by a drying process, which is accompanied with a certain

amount of shrinkage and densification. The resulting sol-gel is usually highly porous

which means it has so many pores on the surface and a high surface area. The

distribution and size of the pores determine the process of the removal of the extra

liquids. There are many ways to implement this. Sometimes, we only need to wait and

the sedimentation will occur, and then we can pour off the extra liquid. Sometimes,

the sol-gel even can become the colloid by itself and the extra liquid will volatilize

into the air. However, many other equipments can be used to accelerate this process,

such as centrifuging or heating [17].

Sol-gel processing is a low-cost technique. Its raw materials are very easy to

fabricate or purchase. There are also few expensive procedures in the sol-gel

fabrication process. It is also a low-temperature technique, making it compatible with

biomolecule immobilization and can be doped with various additives, which usually

will disperse very uniformly in the final product [17].

There are many applications for the sol-gel derived silica materials. The first is

19

in the film engineering. The sol-gel precursor can be deposited on a substrate to form

a film, by either dipping or spinning. As sol-gel derived silica is a bio-compatible

material, it is widely used in the biosensing technique. People usually coat a layer of

sol-gel derived silica as a film on the sensor then coat another bio-recoginition film on

top of the sol-gel. It also can be used to produce a very thin film for the metal oxides.

Sol-gel derived silica material can also be cast into a suitable container with the

desired shape. Thirdly, it can be used to make powders such as, microspheres or

nanospheres. It also has so many other applications in optics, electronics, energy,

space, biosensors, medicine, reactive material, ceramics processing, investment

casting material and separation technology [17].

1.6 Aptamer

Aptamers are single stranded nucleic acid sequences that can bind to non-DNA

or RNA targets. In the biochemical process, it usually binds or interacts with a specific

type of biomolecule and doesn't react with others. DNA aptamers are single stranded

DNA moelecules which have ligand-binding ability and catalytic function. In the

aptamer fabrication engineering, there is usually a large group random sequences in a

pool and the aptamer can be isolated from it (Figure 1.9). Of course, there are also

some natural apatmers which exist in riboswitches.
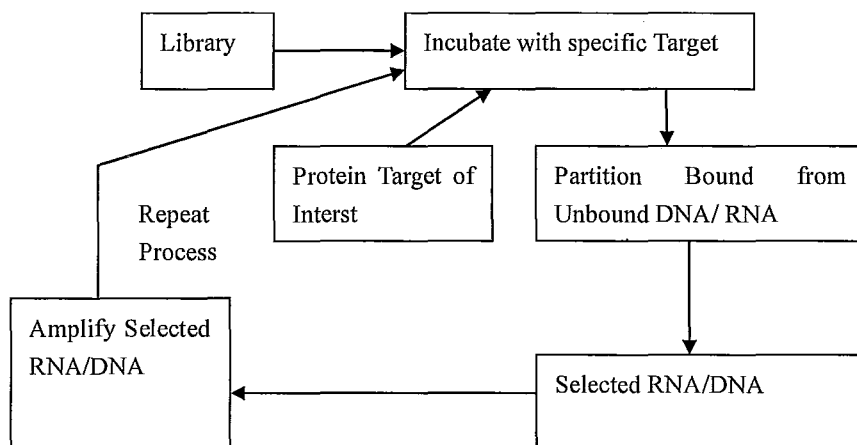
Figure 1.9 The DNA select Process [18]

Nucleic acid aptamers are nucleic acid species. They are usually fabricated by repeating rounds of in vitro selection or equivalently, systematic evolution of ligands by exponential enrichment. In the in vitro selection, aptamers are selected from non-functional RNA or DNA pool. In a standard DNA-oligonucleotide synthesizer a starting pool is first generated. The machine synthesizes an oligonucleotide library with a completely random base-sequence which is flanked by defined primer binding sites. In this process, more than 10^{15} sequences can be synthesized. Then a few molecules with the correct receptor structure will be selected by affinity chromatography or filter binding. The nucleic acid aptamer can bind to various molecular targets such as small molecules, proteins, nucleic acids, and even cells, tissues and organisms. Aptamers are very useful in biochemical and biomedical

engineering because the aptamer usually has high selectivity and only binds or reacts

with a specific type of biomolecule. This is very different from the biomolecules or

antibodies which are used in the previous technique. In addition to its good

recognition properties, aptamers have many other advantages than antibody. For

instance, the aptamer fabrication can be finished completely in a test tube. Its also

have better storage properties and less or no immunogenicity in the medical

applications than antibodies, and can be engineered to produce color change or SPR

on electrochemical responses [18] [19].

2. Motivation

2.1 Motivation for label-free long period grating based biosensor

Nowadays, there is more and more demand for rapid and sensitive bacterial

detection in the environment protection, water treatment and other medical and

environmental applications. Biosensors, which are effective devices to allow such

detection, are becoming the focus of many research groups. Producing a device with

high sensitivity, high selectivity, fast detection speed and low cost is a key issue in the

biosensor research. As discussed above, there are many methods to fabricate the

biosensors, most of which use labels [5]. The label-based biosensor, especially the

fluorescent biosensor, relies on the attachment of tags to biomolecules on the

bioreceptor or the target molecules which may have extra reaction to influence the

result of the experiment. Background influence can also be an issue for the

disadvantage of the label-based biosensor. There are also a good many label-free

biosensors fabricated or reported. However, most of the label-free biosensor are too

expensive and complicated and are hard to commercially fabricate. That is also the

reason that we researched this long period grating based biosensor.

2.2 Motivation for the in-fiber Michelson interferometer structure.

There are several advantages for the in-fiber Michelson interferometer

structure.

Firstly, its size is very small and very portable. The total sensor is a piece of

bare fiber with a pigtail which has a fiber connector. The diameter of the fiber in the

sensor is about 125 um, which is the same with the standard single mode fiber. The

length of the bare fiber where the sensor locates is several centimeters long. The

pigtail which connects to the fiber connecters is also several tens of the centimeters

long. The whole volume of the sensor is very small and portable, which is a great

advantage when it is compared to other biosensors.

Secondly, it works in the reflection mode, not the transmission mode, which

means it only has one port. As we know, the bare fiber is very fragile and can't be bent.

If the sensor has two ports and can't be bent, the only method to immerse the sensor

into the analyte solution is to immerse the whole sensor into it. Using the in-fiber Michelson interferometer structure only needs the sensing head to be immersed into the solution.

Thirdly, this biosensor works at the standard optical communication wavelength. Nowadays, the optical communication is widely used around the world and the optical components in this wavelength are very easy to fabricate and get and the price is also very low. This makes sure the low cost of the fabrication and operation of this sensor system.

Fourthly, this kind of biosensor is fabricated by two parts. The long period grating is fabricated in one piece of the fiber and the gold mirror is coating on another piece of fiber. Then the two parts are spliced together. The bio-recognition film is also coated on the end of fiber and won't touch the long period grating. This gives us a good advantage that the sensing head can be replaced very easily and inexpensively. We only need to fabricate a new sensing head, then cleave the old one and splice the new one. The whole sensor refabrication is not needed. This can greatly save the long period gratings and fiber connectors which is comparatively hard to fabricate.

Fifthly, the Michelson interferometer is a good refractive index change detector. It has the evanescent wave which penetrates into the ambient environment

and can detect some small changes of the ambient refractive index. It is also not hard

to enhance the sensitivity of the optical fiber biosensor by structure modification. In

our past work, there are two methods. The first method is to etch the cladding of the

fiber. This method can achieve a relative high sensitivity but the fabrication technique

is comparatively difficult. The second method is to add a high refractive index overlay

on top of the sensing head. The high refractive index overlay could be polymeric

nano-film or sol-gel derived silica film. The polymeric nano-film can also achieve a

relative high sensitivity but it is not easy to be compatible to the bio-material. The

sol-gel derived silica film can't achieve a so high sensitivity as polymeric nano-film

but it is easy to immobilize the bio-recognition molecules onto it.

2.3 Motivation for sol-gel material and aptamers

As discussed above, a layer of film should be coated on top of the end of the

fiber. It is used to enhance the sensitivity of the label-free LPG biosensor and also

should be a medium to immobilize the aptamer and biomolecules on it. There are so

many film that can be applied in this sensor such as Ta_2O_5 [36], ionic self-assembled

multilayer films [37], Langmuir-Blodgett films [38], polymeric nano-film with silver

particles [35] and sol-gel derived silica film. Each film has its own deposition

technology. For instance Ta_2O_5 film is usually used the sputtering and the ionic

self-assembled multilayer films are usually used the oppositely charged

polyelectrolytes. There are also some other ways such as e-beam evaporation,

molecular-beam expitaxy, chemical vapour deposition and so on, which is the common film growth and deposition technologies in the semiconductor engineering. However, these methods are not suitable for the fiber which is a very thin cylindrical structure. The coating method used for the polymeric nano-film and sol-gel derived silica film is the dipping [30] which is very easy and compatible for the fiber. You just need to immerse the fiber into the prepared solution and then pull it out. Compared with polymeric nano-film, coating of sol-gel is even easier. You don't need to prepare so many solutions and immerse your fiber into different solutions and wait which is the method of polymeric nano-film. You just need one tube of the sol-gel precursor solution and then add the buffer and other additives you want (PEG, gold nano-particle solution) and then dip your fiber into the solution and pull it out at a fixed velocity one time to form a good sol-gel film.

For the sensitivity enhancement, it requires a high refractive index of the overlay film if you only want to coat a thin film layer. A previous student, Pawan Sandhu [35], demonstrated that it can achieve 1.7-2.2 in the refractive index of the polymeric nano-film by adding silver particles. According to the sol-gel film, there are also methods to enhance the sensitivity which is adding gold nano-particles and growing the gold nano-particles. Although the refractive index can't be enhanced very high currently (only can achieve 1.5), it still can enhance some sensitivity by adjusting the refractive index. The sol-gel film also has another property which can complement

the sensitivity. Its surface is not flat as the polymeric nano-film. It is very porous

which means it has a lot of pores on the surface. This property can greatly enhance

surface area over the bare fiber which means more aptamers can be binded on top of

the fiber and enhance the sensitivity.

Another advantage is the sol-gel film is compatible with the bio-materials,

such as aptamer and aptazyme which is very superior over the polymeric nano-film.

That is also the most important reason that we select the sol-gel film in this thesis

other than the polymeric film. The immobilization of bio-sensing molecules such as

aptamer and aptazyme is very easy. We only need to immerse our fiber into several

prepared bio-molecule solutions one by one and incubate the fiber in the solution for

several hours. In this process, there is not any technique difficulties and it is easy to

handle.

3. Research Target

There are several goals of the research. In this project, the whole goal is to

develop a biosensor with short response time, high sensitivity and good selectivity.

But in our work, the first one is to demonstrate there is sensitivity enhancement in the

biosensing when we coat the sol-gel film on top of the fiber when it is compared with

the bare fiber device. Secondly, the aptamer immobilization on the sol-gel film has

been done successfully in the plane slides. In this research work, this should

demonstrate that it also works for the fiber which is a very thin and cylindrical structure. We also need to make sure this binding is not a non-specific binding. Thirdly, the target biomolecule should be binded with the aptamer which is immobilized on the fiber previously successfully and can be reflected in the change of the interference spectrum of the fiber optical biosensor. Fourthly, the aptamer which is immobilized on the fiber is high selectivity. We also need to demonstrate it has the same selectivity and works well when it is immobilized on the fiber. Fifthly, the relationship between concentration and signal (the wavelength shift) also need to be researched.

4. Thesis Structure

The thesis is organized in this way. In Chapter one, it is the background introduction of different kinds of optical biosensors, sol-gel derived silica film and aptamer. The motivation for this research work, research target and thesis structure are also introduced in the first chapter. In Chapter two, the theory analysis and simulation analysis of the long period grating based optical fiber biosensor is introduced. The principle of optical fiber grating first and then the working principle of the in fiber Michelson interferometer are introduced. After that, the way to enhance the sensitivity, the mathematical model of simulation and simulation results is introduced. In Chapter 3, it includes the details of the fabrication of the gold mirror, long period grating, sol-gel derived silica film, the biomolecules which is used in the aptamer immobilization and the aptamers. The detail step of the experiment and experiment

setup is also included. In Chapter 4, the experiment results and discussion are included

in this chapter and there is a conclusion summary and future work considerations in

Chapter 5.

Chapter 2 Theory and Simulation for Long Period Grating based Biosensor

1. Long Period Grating

1.1 Theory of Long Period Grating

Fiber grating is a kind of device which has a periodic refractive index modulation in the core of fiber. There are so many methods to implement this. The most widely used method is to use a UV light passing an amplitude mask to side expose the fiber. As the fiber core, which is Ge doped silica, is photosensitive, the refractive index of the core of the fiber is modulated by the UV light. However, as the cladding of the fiber is not photosensitive, the refractive index of the cladding remains unchanged. The refractive index modulation of the fiber can be expressed as follows:

$$n_1(z) = n_1\{1 + \sigma(z)[1 + m\cos(\frac{2\pi}{\Lambda}z)]\} \tag{2.1}$$

In this expression, n_1 is the refractive index of the fiber core. m, is the refractive index modulation (0<m<1). Λ is the period of the grating, and $\sigma(z)$ is the refractive index modulation envelope. Long Period Grating is grating with a large period, usually several hundred of micrometers to a few millimeters [20] [21] [22].

In the long period grating based biosensor, the core mode is coupled with the co-direction cladding mode. The phase condition of the mode coupling is very important.
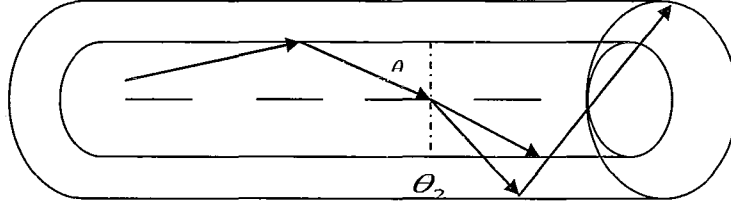
Figure 2.1 The ray of the core- cladding mode coupling

From the diagram above, we can easily get this expression below:

$$n_2 \sin \theta_2 = n_1 \sin \theta_1 + q \frac{\lambda}{\Lambda}$$

(2.2)

In this expression, n_1 is the core refractive index, n_2 is the cladding refractive index, q is the order of diffraction, λ is the wavelength of the light, Λ is the period of the diffraction grating, θ_1 is the angle of incidence, and θ_2 is the angle of diffraction.

When it refers to the long period grating, the q= -1 as the long period grating is a transmission grating. We also can regard the $n_{eff, core} = n_1 \sin\theta_1$, $n_{eff, cladding} = n_2 \sin\theta_2$. In this case, the equation (2.2) can be written as

$$\lambda = (n_{eff}^{core} - n_{eff}^{cl})\Lambda$$

(2.3)

The equation (2.3) is the phase matching condition for the core-cladding mode coupling. As the result of the effective index of the cladding minus the effective index of the core is very small, the period of the grating should be very large. That is why

we need to use the long period grating for the core-cladding mode coupling biosensor.

Equation (2.3) is also a very important expression in the long period grating

fabrication. It can be used to select the period of the amplitude mask which will be

described in the next chapter [23] [24].
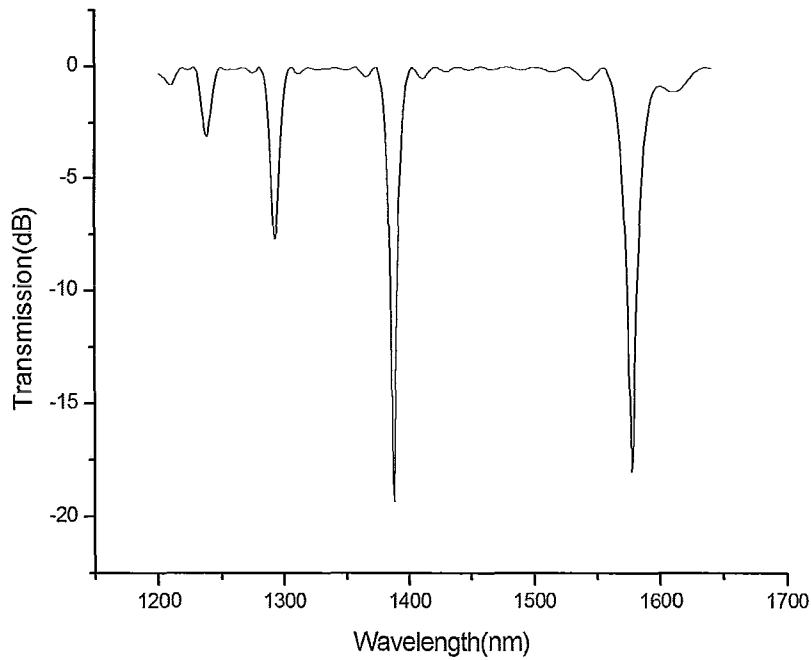

Figure 2.2 Experimental spectrum of the long period grating

1.2 Spectrum of LPG

Figure 2.2 is the an experimental spectrum of the long period grating in the

1200nm-1600nm range. There are five notches shown in the spectrum. They are

according to the HE_{11} mode coupled to HE_{13}, HE_{14}, HE_{15}, HE_{16}, HE_{17} from the left to

the right. We can see the depth of the notches are increased when the order of the mode is increased. This is because the cladding mode field amplitude is increased when the order of the mode is increased.

2. Working Principle of the Long Period Grating Biosensor

2.1 Michelson Interferometer

The idea of the long period grating comes from the Michelson interferometer. The diagram of the standard Michelson Interferometer is as below (Figure 2.3). Michelson interferometer is a very famous device in the optical interference. It is implemented by Alberta Michelson and is used to demonstrate the speed of light is a constant value even using different kinds of inertial frames. This experiment is the famous Michelson- Morley experiment. Its basic principle is very easy to split one beam into two beams and recombine them again.

The system contains two polished mirror, one half-reflection-half-transmission mirror, a photodetector and light source. The light source should be monochromatic. When the light comes out of the light source, it is half reflected and half transmitted by the half silver mirror. The two beams meet the polished mirrors and are reflected. One of the beams directly propagates into the photodetector and the other beam is reflected again by the half silver mirror and recombined with the first beam and cause the interference. The trick is that the coherent light will split into two beams with the

same intensity if it passes a semi-transparent mirror and both beams should be

coherent. The light intensity after the recombination can be expressed as follows:

$$I \propto |E_1|^2 + |E_2|^2 + 2E_1E_2 \cos \delta\phi \qquad (2.4)$$

Mirror M_1

Half Silver
Mirror

Light
Source

Mirror M_2

Detector
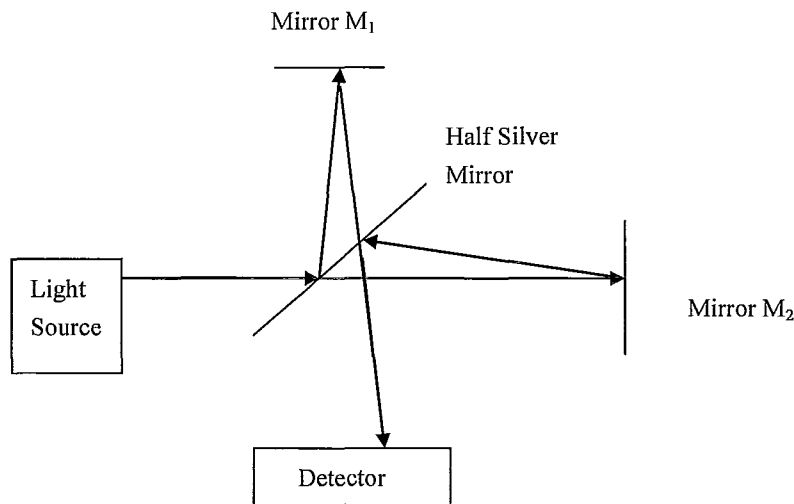
Figure 2.3 Configuration of Michelson Interferometer

The $\delta\phi$ is the phase difference of the two separate beams. In this case, the

intensity of the light after the recombination will be the sinusoidal function of the

phase difference. The phase of each beam is determined by the length of propagation

and the propagation constant of each beam. The propagation constant is related to the

refractive index, so the change of the length of propagation, which is the Michelson

interferometer arm length, or the refractive index will make the wavelength shift in the

interference spectrum. The Michelson interferometer can be used to detect the

refractive index change [25].

2.2 Long Period Grating Based Biosensor

The long period grating is also called the in-fiber Michelson interferometer as it is used the principle of the Michelson interferometer in a standard single mode fiber. The structure of in-fiber Michelson interferometer is very easy which is shown in Figure 2.4. It is a standard fiber with a long period grating which is fabricated by the side-exposure to the UV light method. It also has a very flat gold mirror in the long distance end.

LPG

Gold Mirror

Figure 2.4 Structure of the long period grating based biosensor

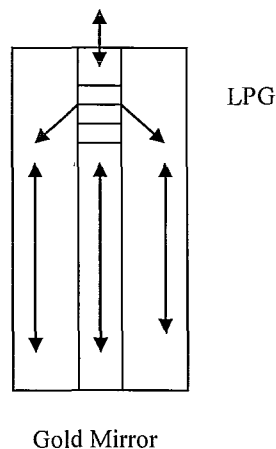This kind of biosensor uses both the core and cladding as the light propagation medium which is like the light propagation arms in the Michelson interferometer. The lengths of the "two arms" are the same as the cladding and the core are in the same length. The long period grating which is inscribed in the fiber works as a beam splitter.

When the light is injected into the fiber core, it meets the long period grating at the

beginning of this sensor. The long period grating is like a beam splitter and split part

of the light of the core mode to the cladding which also can be described as coupling

the core mode HE_{11} to co-directional cladding modes. The light coupled into the

cladding then propagates in the cladding and works as a cladding mode. The coupling

is partial and still part of the light remains in the core and propagates as the form of

HE_{11} in the core. Both the two kinds of beams are reflected by the flat gold mirror

which is in the cleaved long distance end. Based on the reversible effect, the cladding

modes are coupled back to the core when they meet the long period grating again after

the reflection. The two beams are recombined in the core after passing the long period

grating in the second time which causes the interference and we can observe an

interference spectrum in the optical analyzer. The cladding modes have an evanescent

wave penetrating into the ambient environment which is just like a "hand" to touch the

ambient environment. This kind of interference spectrum depends on the optical

properties of all the layers that participate into the light modes propagation. If the

optical properties of the layers are changed, the effective index of the cladding modes

will be changed which will cause the phase difference condition to change and change

the constructive and destructive of interference spectrum. At last, we can see the

wavelength shift in the spectrum [26].

The obvious advantage of the in-fiber Michelson interferometer to the

traditional Michelson interferometer is the portable structure and easy fabrication. The traditional Michelson interferometer which is described above has two separated light propagation arms. One arm is usually vertical to the other arm. It also contains a bunch of other components such as three separated mirrors. However, the in-fiber Michelson interferometer, which is the structure of our long period grating based biosensor, only has one arm to guide two beams. One part of arm, fiber core, guide one beam and the other part of the arm, fiber cladding, guide another beam [26].

Among all the light modes, the core mode HE_{11} is supported totally by the fiber core which is isolated from the surrounding ambient in a single mode fiber, so the core mode HE_{11} is not sensitive to the refractive index change of the ambient environment at all. However, the cladding modes are not totally supported by the fiber core, so it has an evanescent wave penetrating into the ambient environment and can feel the refractive index changes in the ambient. Thus, the refractive index change of the ambient can make the changes of the effective index of the cladding mode and then make wavelength shift of the spectrum of the biosensor. Sometimes, we also change the wavelength shift to effective index change or phase change in order to make a baseline for all the different devices. As the core mode is isolated from the ambient, the effective index change only refers to the cladding modes. In the output biosensor spectrum, the phase differences of the two deep peaks are given by this equations.

$$\Delta\phi = [2(m+1)+1-(2m+1)]\pi = 2\pi L\Delta n(\frac{1}{\lambda_1}-\frac{1}{\lambda_2}) \qquad (2.5)$$

The difference in refractive index between two path is $\Delta n = [(\lambda_1\lambda_2)/(\Delta\lambda L)]$. L is the traversed length by two waves and λ_1, λ_2 ar e the wavelength of the two adjacent peaks. The fringe spacing is much smaller than the wavelength we are using, so we can get the following equation:

$$\Delta n_{eff}^{cladding} \approx \frac{\lambda}{\Delta\lambda L_{imm}}\delta\lambda \qquad (2.6)$$

In this equation, λ is the wavelength of a peak in the output spectrum, $\delta\lambda$ is the wavelength shift in the output spectrum. $\Delta\lambda$ is the spacing of two peaks in the output spectrum which is dependent on the length of the biosensor and L_{imm} is the immersion depth of the biosensor. λ $\Delta\lambda$ and L_{imm} ar e controlled by the fabrication technique and experimental operation and is usually fixed , so the effective index change of cladding modes will be directly influence the wavelength shift [23] [24].

3. Numerical Simulation Method

Simulation is a very important step in the device design. The simulation is based on the mode solve method. It calculates the effective index of the cladding modes according to different parameters to research how the effective indices change of the cladding modes. In our experiments, we put sol-gel on top of the fiber, so there are four layers for the system, ambient environment, sol-gel film, fiber cladding and fiber core. The mode is considered as a four-layer structure. The goal of the simulation

is to determine the refractive index and thickness of the sol-gel film which can make

the device in the high sensitivity working condition. In this simulation, there are three

parameters to vary, which are the refractive index and thickness of sol-gel film and the

refractive index of the ambient environment.

The mathematical model for the simulation is borrowed from Yeh's work.

From the Maxwell equation, we can get the electric and magnetic fields as follows:

$$\nabla \times \vec{E} = -\mu_0 \frac{\partial \vec{H}}{\partial t}$$

$$\nabla \times \vec{H} = \mu_0 \varepsilon_0 \varepsilon_r \frac{\partial \vec{E}}{\partial t} \qquad (2.7)$$

The light wave is usually the plane wave in the Z direction, so we can write:

$$\vec{E} = \vec{E}(r,\theta)e^{i(\omega t-\beta z)}$$

$$\vec{H} = \vec{H}(r,\theta)e^{i(\omega t-\beta z)} \qquad (2.8)$$

The r is the transverse radius and θ is the azimuth, β is the propagation constant

of a mode. It equals to $(2\pi n_{eff})/\lambda$. Here, the n_{eff} is the effective index of the mode.

From the four equations above, we can easily get the wave equations.

$$\nabla^2 \vec{E} = -\varepsilon_0 \mu_0 n^2 \omega \vec{E}$$

$$\nabla^2 \vec{H} = -\varepsilon_0 \mu_0 n^2 \omega \vec{H} \qquad (2.9)$$

As we want to solve these wave equations, we need to change this equation 2.9 into

the cylindrical coordinates. We can use the method of separating the form of the

solutions. We can write $E_z(r,\theta)=E_z(r)e^{iv\theta}$ and $H_z(r,\theta)=H_z(r)e^{iv\theta}$. Here, v is an

integer for the z components. We can get:

$$\frac{\partial^2 E_z(r)}{\partial r^2}+\frac{1}{r}\frac{\partial E_z(r)}{\partial r}+(q^2-\frac{v^2}{r^2})E_z(r)=0$$

$$\frac{\partial^2 H_z(r)}{\partial r^2}+\frac{1}{r}\frac{\partial H_z(r)}{\partial r}+(q^2-\frac{v^2}{r^2})H_z(r)=0 \qquad (2.10)$$

The equations above are the Bessel Equations. This is the equation what we will solve

in the simulation. It will have Bessel solutions if the q^2 is larger than zero and have the

modified Bessel solutions if the q^2 is smaller than zero.

$$E_Z(r)=AJ_v(qr)+BY_v(qr)$$
$$H_Z(r)=CJ_v(qr)+DY_v(qr) \qquad (2.11)$$

and

$$E_Z(r)=AJ(\;w\!\!\!/r\;)\qquad \beta(\;$$
$$H_Z(r)=CJ(\;w\!\!\!/r\;)\qquad D(\; \qquad (2.12)$$

If we use the Maxwell equations, we can write this to r and θ components of the

electrical and magnetic fields in terms of the z-components:

$$E_r(r,\theta)=-\frac{i}{q^2}(\beta\frac{\partial E_z(r,\theta)}{\partial r}+\frac{\mu_0\omega}{r}\frac{\partial H_z(r,\theta)}{\partial\theta}$$

$$H_r(r,\theta)=-\frac{i}{q^2}(\beta\frac{\partial H_z(r,\theta)}{\partial r}-\frac{\varepsilon_0 n^2\omega}{r}\frac{\partial E_z(r,\theta)}{\partial\theta}$$

$$E_\theta(r,\theta)=-\frac{i}{q^2}(\frac{\beta}{r}\frac{\partial E_z(r,\theta)}{\partial r}-\mu_0\omega\frac{\partial H_z(r,\theta)}{\partial r} \qquad (2.13)$$

$$H_\theta(r,\theta)=-\frac{i}{q^2}(\frac{\beta}{r}\frac{\partial H_z(r,\theta)}{\partial\theta}+\varepsilon_0 n^2\omega\frac{\partial E_z(r,\theta)}{\partial r}$$

In order to get the solution in the simulation, we can consider a field strength vector

consisting of the tangential components of the EM wave, H_z, H_θ, E_z, E_θ:

$$\begin{bmatrix} E_z(r) \\ H_z(r) \\ E_\theta(r) \\ H_\theta(r) \end{bmatrix} = F_i(r) \tag{2.14}$$

Here, the i means the ith layer. We can use COE$_i$ to substitute the vector coefficient in

the ith layer:

$$COE_i = \begin{bmatrix} A_i \\ B_i \\ C_i \\ D_i \end{bmatrix} \tag{2.15}$$

The field strength vector can be expressed as follows:

$$\begin{bmatrix} E_z(r) \\ H_z(r) \\ E_\theta(r) \\ H_\theta(r) \end{bmatrix} = \begin{bmatrix} J_v(u_i r) & Y_v(u_i r) & 0 & 0 \\ 0 & 0 & J_v(u_i r) & Y_v(u_i r) \\ \dfrac{\beta}{\mu_i^2 r} J_v(u_i r) & \dfrac{\beta}{\mu_i^2 r} Y_v(u_i r) & \dfrac{jk_0 z}{\mu_i} J'_v(u_i r) & \dfrac{jk_0 z}{\mu_i} Y'_v(u_i r) \\ -\dfrac{jk_0 n_i^2}{\mu_i} J'_v(u_i r) & -\dfrac{jk_0 n_i^2}{\mu_i} Y'_v(u_i r) & \dfrac{j\beta}{\mu_i^2 r} J_v(u_i r) & \dfrac{j\beta}{\mu_i^2 r} Y_v(u_i r) \end{bmatrix} \begin{bmatrix} A_i \\ B_i \\ C_i \\ D_i \end{bmatrix} \tag{2.16}$$

We can use M$_i$ to substitute the first bracket at the right of the Equation 2.16:

$$M_i = \begin{bmatrix} J_v(u_i r) & Y_v(u_i r) & 0 & 0 \\ 0 & 0 & J_v(u_i r) & Y_v(u_i r) \\ \dfrac{\beta}{\mu_i^2 r} J_v(u_i r) & \dfrac{\beta}{\mu_i^2 r} Y_v(u_i r) & \dfrac{jk_0 z}{\mu_i} J'_v(u_i r) & \dfrac{jk_0 z}{\mu_i} Y'_v(u_i r) \\ -\dfrac{jk_0 n_i^2}{\mu_i} J'_v(u_i r) & -\dfrac{jk_0 n_i^2}{\mu_i} Y'_v(u_i r) & \dfrac{j\beta}{\mu_i^2 r} J_v(u_i r) & \dfrac{j\beta}{\mu_i^2 r} Y_v(u_i r) \end{bmatrix} \tag{2.17}$$

So, we can write Equation 2.17 as:

$$F(r) = M_i \cdot COE_i \tag{2.18}$$

At the interface of the ith layer and the (i-1)th layer,

$$F_i(r_i) = M_i(r_i) . COE_i$$

$$F_{i-1}(r_{i-1}) = M_i(r_{i-1}) . COE_i \qquad (2.19)$$

Then we can get:

$$F_i(r_i) = M_i(r_i) \, M_i^{-1}(r_{i-1}) \, F_i(r_{i-1}) \qquad (2.20)$$

In order to simplify the equation, we can use a new matrix $T(r_i, r_{i-1})$ to substitute

$M_i(r_i) \, M_i^{-1}(r_{i-1})$, which is:

$$F_i(r_i) = T_i(r_i, r_{i-1}) \, F_i(r_{i-1}) \qquad (2.21)$$

Next, we can use the boundary condition. It should be continuous in the interface,

which means:

$$F_{i+1}(r_i) = F_i(r_i) \qquad (2.22)$$

So, we can write Equation 2.21 as:

$$F(r_i) = T_i(r_i, r_{i-1}) \, F(r_{i-1}) \qquad (2.23)$$

We can write a lot of such equations:

$$F(r_{n-1}) = T_{n-1}(r_{n-1}, r_{n-2}) \, F(r_{n-2})$$

$$F(r_{n-2}) = T_{n-2}(r_{n-2}, r_{n-3}) \, F(r_{n-3})$$

$$\ldots.$$

$$F(r_2) = T_2(r_2, r_1) \, F(r_1) \qquad (2.24)$$

Then we can combine these equations and get:

$$F(r_{n-1}) = T_{n-1} \, T_{n-2} \ldots T_2 \, F(r_1) \qquad (2.25)$$

We can use T to substitute $T_{n-1} \, T_{n-2} \ldots T_2$ and get:

$$F(r_{n-1}) = T \, F(r_1) \tag{2.26}$$

Based on the natural of the second kind Bessel function, $Y_v(ur)$ will approaches to

∞, when r approaches to zero. In this case, the field coefficient for this term should

also be zero, which means B_1, $D_1 = 0$. So Equation 2.16 can be expressed as:

$$
\begin{bmatrix} E_z(r) \\ H_z(r) \\ E_\theta(r) \\ H_\theta(r) \end{bmatrix} =
\begin{bmatrix}
J_v(u_i r) & 0 & 0 & 0 \\
0 & 0 & J_v(u_i r) & 0 \\
\dfrac{\beta}{\mu_i^2 r} J_v(u_i r) & 0 & \dfrac{jk_0 z}{\mu_i} J'_v(u_i r) & 0 \\
-\dfrac{jk_0 n_i^2}{\mu_i} J'_v(u_i r) & 0 & \dfrac{j\beta}{\mu_i^2 r} J_v(u_i r) & 0
\end{bmatrix}
\begin{bmatrix} A_i \\ 0 \\ C_i \\ 0_i \end{bmatrix} \tag{2.27}
$$

The above is the inner condition of the system. When it refers to the outer place of the

system, the radius becomes large and the electrical field becomes zero. In this case,

the coefficient of the $I_v(ur)$ must be zero, which means $B_i = D_i = 0$, so we can express

the interface of the most outer layer as follows:

$$
\begin{bmatrix} E_z(r_{n-1}) \\ H_z(r_{n-1}) \\ E_\theta(r_{n-1}) \\ H_\theta(r_{n-1}) \end{bmatrix} =
\begin{bmatrix}
K_v(w r_{n-1}) & 0 & 0 & 0 \\
0 & 0 & K_v(w r_{n-1}) & 0 \\
-\dfrac{\beta}{w^2 r_{n-1}} K_v(w r_{n-1}) & 0 & \dfrac{-jk_0 z}{w} K'_v(w r_{n-1}) & 0 \\
-\dfrac{jk_0 n_n^2}{w z} K'_v(w r_{n-1}) & 0 & -\dfrac{\beta}{w^2 r_{n-1}} K_v(w r_{n-1}) & 0
\end{bmatrix}
\begin{bmatrix} A_n \\ 0 \\ C_n \\ 0 \end{bmatrix} \tag{2.28}
$$

From Equation 2.27, Equation 2.28 and Equation 2.26 we can get:

$$
\begin{bmatrix}
K_v(wr_{n-1}) & 0 & 0 & 0 \\
0 & 0 & K_v(wr_{n-1}) & 0 \\
-\dfrac{\beta}{w^2 r_{n-1}}K_v(wr_{n-1}) & 0 & \dfrac{-jk_0 z}{w}K'_v(wr_{n-1}) & 0 \\
-\dfrac{jk_0 n_n^2}{wz}K'_v(wr_{n-1}) & 0 & -\dfrac{\beta}{w^2 r_{n-1}}K_v(wr_{n-1}) & 0
\end{bmatrix}
\begin{bmatrix} A_n \\ 0 \\ C_n \\ 0 \end{bmatrix} =
$$

$$
T
\begin{bmatrix}
J_v(u_i r) & 0 & 0 & 0 \\
0 & 0 & J_v(u_i r) & 0 \\
\dfrac{\beta}{\mu_i^2 r}J_v(u_i r) & 0 & \dfrac{jk_0 z}{\mu_i}J'_v(u_i r) & 0 \\
-\dfrac{jk_0 n_i^2}{\mu_i}J'_v(u_i r) & 0 & \dfrac{j\beta}{\mu_i^2 r}J_v(u_i r) & 0
\end{bmatrix}
\begin{bmatrix} A_1 \\ 0 \\ C_1 \\ 0 \end{bmatrix}
\tag{2.29}
$$

We can use M to substitute the first matrix in the right of the equation. As the second

and the fourth column are also equal to zero, we can write the new matrix MT as:

$$
MT =
\begin{bmatrix}
MT_{11} & 0 & MT_{13} & 0 \\
MT_{21} & 0 & MT_{23} & 0 \\
MT_{31} & 0 & MT_{33} & 0 \\
MT_{41} & 0 & MT_{43} & 0
\end{bmatrix}
\tag{2.30}
$$

So, Equation 2.29 can be written as:

$$
\begin{bmatrix}
K_v(wr_{n-1}) & 0 & 0 & 0 \\
0 & 0 & K_v(wr_{n-1}) & 0 \\
-\dfrac{\beta}{w^2 r_{n-1}}K_v(wr_{n-1}) & 0 & \dfrac{-jk_0 z}{w}K'_v(wr_{n-1}) & 0 \\
-\dfrac{jk_0 n_n^2}{wz}K'_v(wr_{n-1}) & 0 & -\dfrac{\beta}{w^2 r_{n-1}}K_v(wr_{n-1}) & 0
\end{bmatrix}
\begin{bmatrix} A_n \\ 0 \\ C_n \\ 0 \end{bmatrix} =
$$

$$
\begin{bmatrix}
MT_{11} & 0 & MT_{13} & 0 \\
MT_{21} & 0 & MT_{23} & 0 \\
MT_{31} & 0 & MT_{33} & 0 \\
MT_{41} & 0 & MT_{43} & 0
\end{bmatrix}
\begin{bmatrix} A_1 \\ 0 \\ C_1 \\ 0 \end{bmatrix}
\tag{2.31}
$$

Then we can change the matrix to several equations:

$$MT_{11}A_1 + MT_{13}C_1 - K_v(wr_{n-1})\,A_n + 0 = 0$$

$$MT_{21}A_1 + MT_{23}C_1 + 0 - K_v(wr_{n-1})\,C_n = 0$$

$$MT_{31}A_1 + MT_{33}C_1 + \frac{\beta}{w^2 r_{n-1}} K_v(wr_{n-1})A_n + \frac{jk_0 z}{w} K'_v(wr_{n-1})C_n = 0$$

$$MT_{31}A_1 + MT_{33}C_1 - \frac{jk_0 n_n^2}{wz} K'_v(wr_{n-1})A_n + \frac{\beta}{w^2 r_{n-1}} K(wr_{n-1})C_n = 0$$

(2.32)

So what we will solve is (A_1, C_1, A_n, C_n). In order to have non-trivial solutions, the determinant matrix should be zero:

$$\begin{bmatrix} MT_{11} & MT_{31} & -K_v(wr_{n-1}) & 0 \\ MT_{12} & MT_{32} & 0 & -K_v(wr_{n-1}) \\ MT_{13} & MT_{33} & \dfrac{\beta}{w^2 r_{n-1}} K_v(wr_{n-1}) & \dfrac{jk_0 z}{w} K'_v(wr_{n-1}) \\ MT_{14} & MT_{34} & -\dfrac{jk_0 n_n^2}{wz} K'_v(wr_{n-1}) & \dfrac{\beta}{w^2 r_{n-1}} K(wr_{n-1}) \end{bmatrix} = 0 \qquad (2.33)$$

It is the eigenvalue equation of the multilayer optical fiber based on a full vector model. We can solve this equation to calculate the effective indices of cladding modes. When the effective indices have been got in the simulation, we can use them to calculate other unknown values such as the coefficient of electrical field in each layer [27].

4. Sensitivity Enhancement

Although the long period grating based biosensor can detect some refractive index change, the sensitivity is also very low especially in the low ambient refractive index range. The sensitivity can be increased when the ambient refractive index is increased (but the refractive index should be lower than the refractive index of the cladding), but we want to increase the sensitivity in the whole range of the ambient

refractive index. In the past work, there are two methods to enhance the sensitivity, cladding etching [28] [29] and adding an overlay on top of the sensing head of the fiber. The cladding etching usually needs the hydrogen fluoride which is a very dangerous chemical. The technique is also complicated. The overlay adding work has also been done. A polymeric nano-film with silver gold nano-particles were added on top of the fiber and got a sensitivity enhancement. In our work, a bio-compatible sol-gel derived silica film is used for the aptamer immobilization. Note that the sol-gel film also can work as a sensitivity enhancement overlay film.

The overlay film coating for sensitivity enhancement uses an optical phenomenon [30] called the mode reorganization. When this phenomenon occurs, the amplitude of the evanescent wave is greatly enhanced, so this can be used to enhance the sensitivity of the evanescent wave biosensor both interferometer style and non-interferometer style. Before the mode reorganization occurs, we usually need to coat a high refractive index overlay onto the fiber. As the refractive index of the overlay is usually very high and the thickness of the overlay film is usually very low, it is like a deep but narrow waveguide. If the refractive index and thickness of the overlay film matches well, the overlay film can become a single mode waveguide and totally support the previous lowest order cladding mode which is HE_{12} in our device. Once the lowest order cladding mode transit to the overlay film, other cladding modes will occur, and the energy and effective index will be reorganized. It usually occurs

like this: the effective index of the higher order cladding mode will shift to the next

neighbor lower mode to compensate and redistribute the mode energy. The condition

for mode reorganization has been researched by the computer simulation. Figure 2.5

shows the mode reorganization condition when the refractive index of the overlay film

is equal to 1.65 and 1.75. In the simulation, we set the radius of the fiber core as

4.15um, the radius of the fiber cladding as 62.5um, refractive index of the fiber

cladding as 1.440240, refractive index of the fiber core 1.448933 and the wavelength

of the light at 1550nm. The overlay thickness is set as a variable value, starting from 0

and ending at more than 1000nm. The modes which are simulated is HE_{11}, HE_{12}, HE_{16}

HE_{18} and HE_{19}.

When the refractive index is equal to 1.65 or 1.75, we both can see the mode

reorganization range in the simulation figure. When the refractive index is equal to

1.65, the overlay thickness which can cause the mode reorganization is about 250nm.

However, when the refractive index is equal to 1.75, there are two areas in the mode

reorganization area, the first is about 200nm and the second is about 1000nm. We can

also find that the thickness will be small to cause the mode reorganization if the

refractive index of the overlay is large and there will be more areas for the mode

reorganization if the refractive index is high. Of course, we can enhance the thickness

to cause the mode reorganization if we are unable to enhance the refractive index.

However, if the overlay thickness is too large, the evanescent wave will decay mostly

in the overlay and can't penetrate into the ambient even though it has large amplitude.

The mode reorganization is important for the sensitivity enhancement. Consider the critical condition of the mode reorganization, which is the lowest cladding mode mostly guided by the overlay film but not totally. The remaining cladding modes will have a greatly evanescent wave enhancement which can be shown by the simulation results (Figure 2.6). The second graph is a zoom-in graph of the first one in the fiber surface area. In this simulation, the thickness is fixed at 200nm which is similar to the thickness of sol-gel film we used.
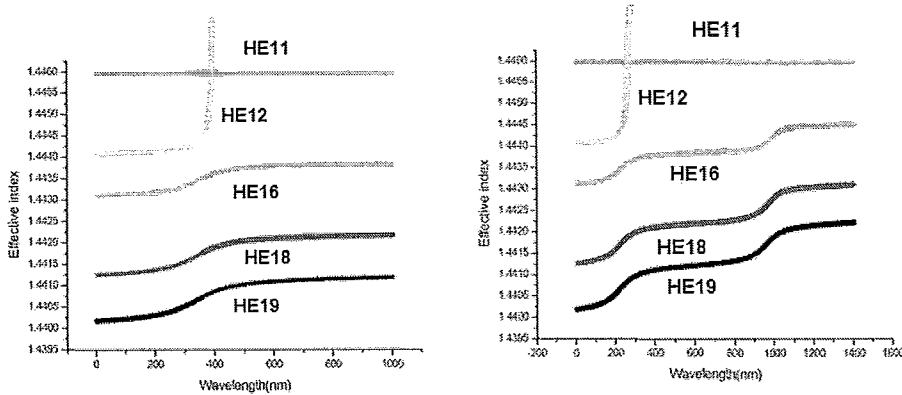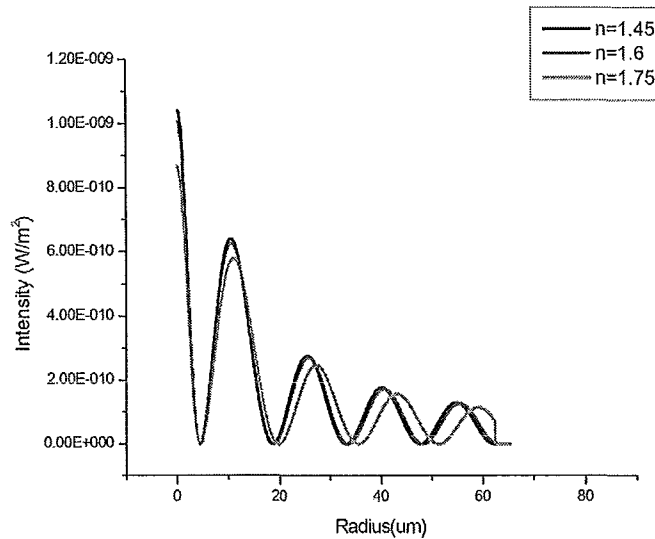

Figure 2.5 Simulation of the mode reorganization condition

The mode we used is the HE_{18} which is the highest order mode and have the largest sensitivity. We can see clearly from the figure: When the refractive index of the overlay film is very low, the amplitude of the evanescent wave is also very small. The overlay film can suck some light out of the cladding but is not sufficient to support it. It is also not enough to change the field distribution of the cladding modes and their

effective indices, which is the condition of the refractive index of the overlay film as
1.45 and 1.6. The amplitude of the evanescent wave is also very small. However,
when it comes to 1.75, which is in the mode reorganization area, we can see the
amplitude of the evanescent wave is greatly enhanced. When the refractive index and
thickness of the overlay film can make the fiber works in the mode reorganization
condition, the overlay film works as a waveguide that can draw much of the light into
itself but can't support the wave totally in itself. As the high existence of the cladding
mode within the overlay and its neighboring ambient, the biosensor will be highly
sensitive to the ambient refractive index change.   We also can see much larger
amplitude of the evanescent wave in the condition of refractive index of 1.75.

(a)
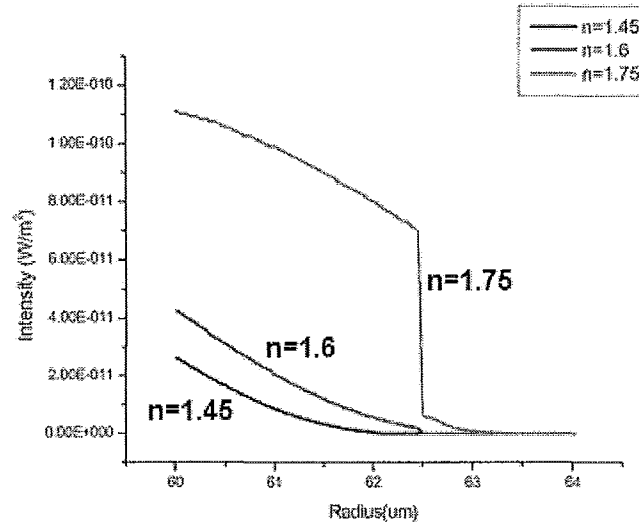
(b)

Figure 2.6   Simulation Results for the evanescent wave amplitude in and out of the mode

reorganization. (b) is a zoom-in area of the fiber surface of (a)

In order to better demonstrate that the film which makes the fiber to work in

the mode reorganization area has the better sensitivity, we simulated the device

performance in Figure 2.7. In Figure 2.7, the y- axis is the effective index change and

x-axis is the ambient refractive index. In this simulation, the thickness of this film is

set at 250nm which is similar to the sol-gel film used in my experiment. We can see

the results from the figure. The bare fiber device sensitivity is very small. Even though

the ambient refractive index increases to more than 1.4, the effective index change is

also very small. When we add a high refractive index overlay onto the fiber, the

sensitivity is greatly enhanced. When the refractive index is 1.55, the sensitivity is

also enhanced a little even though it is still a little far from the sensitivity requirements

which we simulated above (n=1.75). When the refractive index is increased, the

sensitivity is also increased. When the refractive index is increased to 1.75 which is in

the mode reorganization range in our simulation above, the sensitivity is greatly

enhanced. The simulation results obviously show that the sensitivity is enhanced about

2 folds when the refractive index is equal to 1.55. It is enhanced about 9 folds and 14

folds when the refractive index of the overlay film is about 1.65 and 1.75.

So, based on the results of the simulation, n=1.75 is set as the target. Even

though the refractive index of sol-gel film is hard to enhance to a high value, we need

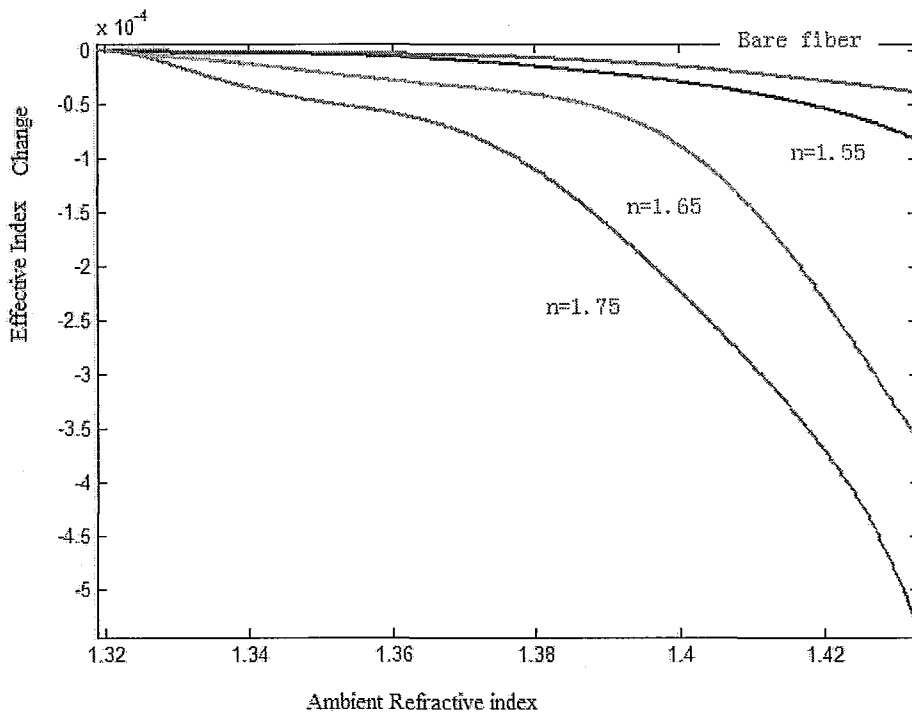to enhance it to around 1.55 at least.

Figure 2.7 Simulation results of the device performance

Chapter 3. Fabrication and Experiment

1. Fabrication of In-Fiber Michelson Interferometer Biosensor

1.1 Long Period Grating Fabrication

In the long period grating fabrication, we usually firstly need to load some fibers (Corning SMF 28) in a hydrogen atmosphere for two weeks at 120 bar. In this step, the hydrogen will diffuse into the fibers and make the fibers photosensitive. To begin the LPG fabrication, the fibers away are removed from the hydrogen and put into a fridge at -36° C and the fibers can be used for about one week. The fibers with hydrogen loaded can't be stored in the room temperature as the hydrogen may spread into the air and the fibers lose photosensitivity [31].

Long period grating fabrication utilized a splicing machine, jump fiber connector, bare fiber clamp, broadband source and optical spectrum analyzer (OSA). Before fabrication, the OSA is calibrated by recording the original optical spectrum of the broadband source. To fabricate the LPG, one end of the fiber is spliced with the jump fiber connector and connected it to the broadband source. Then a fiber stripper is then used to strip the jacket of the fiber and open a window for UV irradiation. The length of the long period grating is determined by the length of the amplitude mask. In our work, we set it at 2.5 cm. After that, the fiber is fixed on the holder of the optical grating writing system. The distance between the fiber and the amplitude mask and the

position of the fiber are adjusted in order to make sure the UV light is exposed on the

fiber. Another end of the fiber can be inserted into the bare fiber clamp and is

connected to the optical spectrum analyzer to obtain another optical spectrum. This

spectrum subtracted the original spectrum of the broadband source to give the

spectrum of the LPG. Figure 2.1 shows the experimental setup of the optical grating
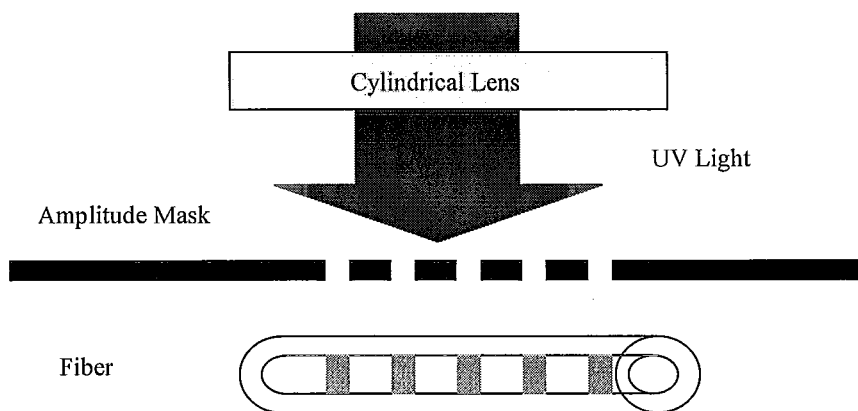
writing system.

Figure 3.1 Schematic Diagram of the LPG fabrication system

The UV laser is a Excimer laser(GSI Lumonics IPEX 848) with a wavelength

at 248nm. In our fabrication, we usually set the voltage at 30 kV and the frequency at

20 Hz to obtain an energy at above 260mJ/pulse.

When the light passes the amplitude mask, some of the light will be blocked

by the mask and the rest will be radiated on the bare optical fiber which is located on

the holder behind the mask. When the fiber is exposed on the UV light, the refractive

index of the fiber core will be modulated and we will get a periodical refractive index

modulation fiber which is also called the in-fiber grating.

According to the theory introduced in the Chapter 2, it satisfies the following

phase matching condition when the core mode is coupled to the co-propagating

cladding mode [22]

$$\lambda = (n_{eff}^{core} - n_{eff}^{cl})\Lambda, \tag{3.1}$$

Where λ is the coupling wavelength and Λ is the grating period. n_{eff}^{core} is the

effective index of the core mode and n_{eff}^{cl} is the effective index of the cladding mode.

In this equation, we can calculate the best period of the amplitude mask. In the work,

the wavelength is around the 1565 nm. The effective index of the core mode at this

wavelength is about 1.4461 and the effective index of the HE_{18} mode is about 1.4411.

The grating period is about 313 um. An amplitude mask with period of 310 um was

used in this work as there is no mask whose period is exactly 313 um.

As the fiber is side exposed in the UV beam, we will see the spectrum

evolution during the LPG fabrication process. Several notches will be observed in

different areas in the spectrum and the notch will grow deeper and move to a longer

wavelength in this process. When the notch is in the right place and right depth, the

process can be stopped. In our case, the depth of the notch is usually set at a little

more than 3 dB, usually at 5-6dB, as the LPG is used as a beam splitter. Too deep a

notch is not good as there will be too much light be coupled into the cladding and only

a little will be left in the core. The 3-dB bandwidth is usually 20-30 nm as we want the

beam splitter to works over the whole range of the spectrum (always 10-20 nm). The

spectrum of one long period grating is shown in Figure 3.2. After all the work has

been done, the long period grating should be put in the oven to be heated for 12 hours

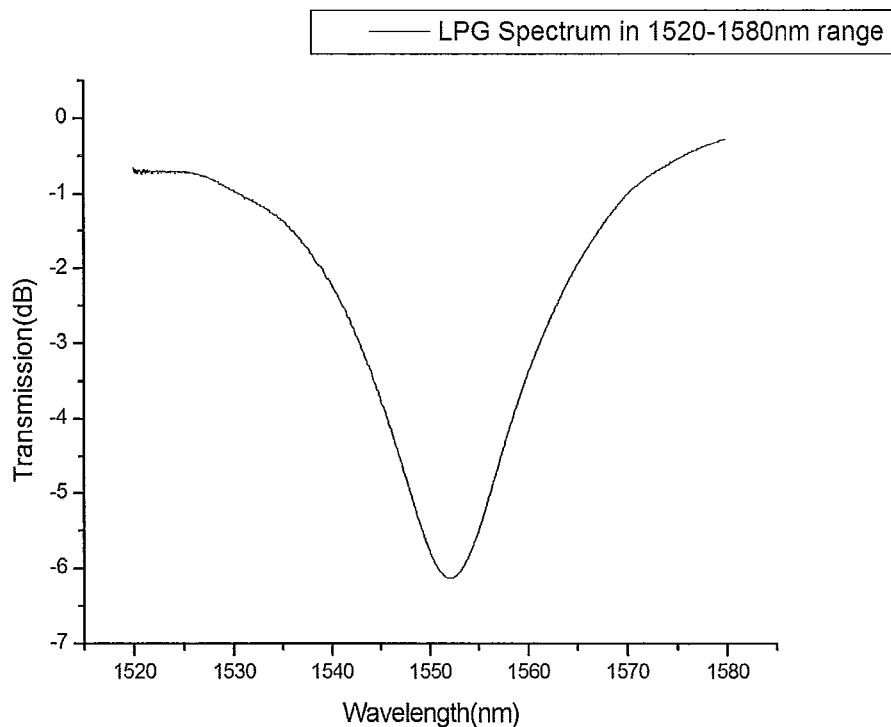at 110 centigrades to remove extra H_2 and set the grating.

Figure 3.2 LPG spectrum

1.2 Gold Mirror Fabrication

After the fabrication of the LPG, the piece of fiber with a gold mirror at the

distal end, also called the fiber sensor cavity, was fabricated. In this fabrication, several hundred of 10 centimeter long pieces of fiber (Corning SMF 28) were fabricated. One end of these pieces of fiber is stripped by the fiber stripper to remove the plastic protection jacket. Then the ends of pieces of fiber which are stripped in the previous step are immersed in a photoresist to form a layer of photoresist on top of the bare fiber. The photoresist used in this work is S1808, which will form a thin layer and is not hard to cleave. Then the fibers are sent to the oven to be heated for more than 3 hours at 110 centigrades. In this step, the photoresist layer on top of the fiber will be hardened. After that, a fiber cleaver is used to cleave the fiber end with photoresist layer, so the side of the fiber will be still coated by photoresist layer and the cross section of the fiber will be exposed in the open air.

After all the previous steps are finished, 36 fiber tips with selected flat end were inserted into 9 glass tubes holder and loaded in the chamber of an e-beam evaporation machine to do the metallization. In the metallization work, a layer of 20nm Cr is first coated on the fiber which is used as an adhesion layer at the speed of 0.08nm/sec. After that, a layer of 300nm gold is coated on top of the Cr layer, which works as a reflection layer, at the speed of 0.1nm/sec. When the metallization work is finished, the fiber tips are put into the acetone. The photoresist is dissolved into the acetone and the gold and Cr which is deposited on top of the photoresist is also taken off from the fiber. As the photoresist is all on the side of the fiber, the gold and Cr

which is on the side of the fiber is taken off and only the gold and Cr which is coated

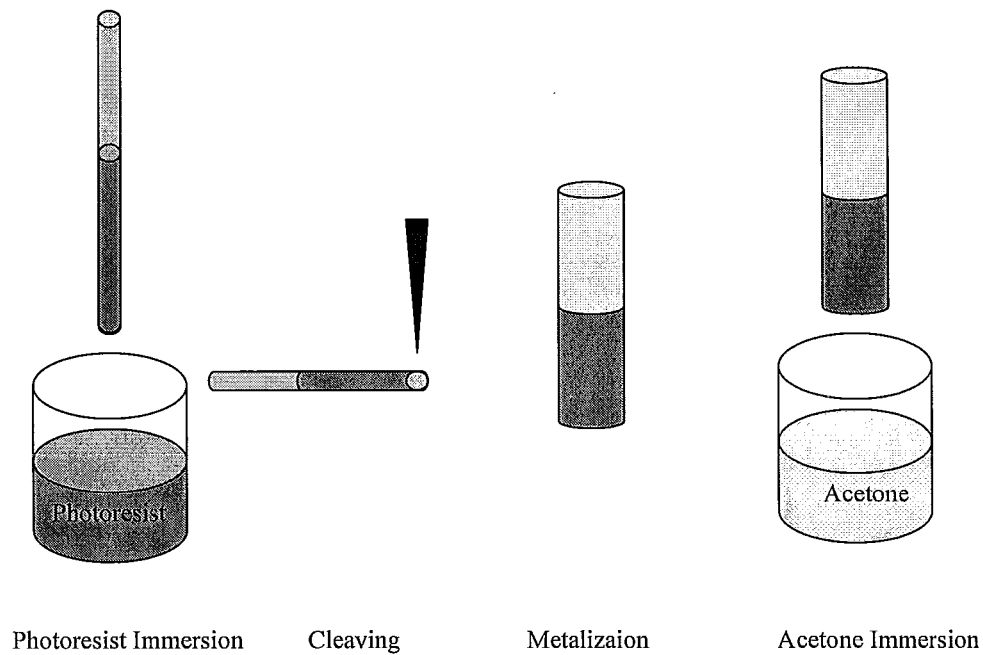at the cross section of the fiber is left. The steps are shown in Figure 2.3

Photoresist Immersion   Cleaving   Metalizaion   Acetone Immersion

Figure 3.3 Steps for the gold mirror at the long distance end of the fiber fabrication

2 Preparation of Sol-gel Derived Silica Film

2.1 Standard Sol-gel Film Preparation

In this work, the sol-gel precursor is prepared by three kinds of materials,

sodium silicate solution, cleaned Dowex, which is an ion exchange of resin, and

Mili-Q water. The dowex is acidic and will generate H^+ in the water and the sodium

silicate is alkaline in the solution. When we mixed the three together, the following

reaction occurs:

$$Si(ONa)_4 + H^+ \xrightarrow{\text{Ion Exchange Resin}} Si(OH)_4 + Na^+ \qquad (3.2)$$
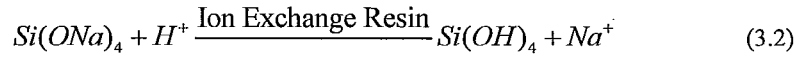
The pH can be adjusted by changing the amount of sodium silicate and cleaned dowex. It is best if the pH is around 4 after this step. In our experiment, we use 10mL of Mili-Q water, 5.5g of cleaned dowex and 2.59g sodium silicate. The three materials were mixed with stirring for 1 minute and then filtered twice. The first time is using the filter paper to filter the dowex and the second time is using 0.45um filter to filter other byproducts. After the sol-gel precursor is prepared, it should be stored on ice and can be used over the next 6 hours [32].

To prepare the sol for dipcasting the sol-gel precursor is mixed with Polyethylene glycol (PEG), 4-(2-hydroxyethyl)-1-piperazineethanesulfonic acid (HEPES) and Mili-Q water. The molecular weight and amount of PEG added in the mixture influences the size of the pores on the sol-gel surface. HEPES works as a buffer in this process. In our work, we add the sol-gel precursor, 200mM HEPES + 20% PEG (10kD) mixture with pH 7.6 and Mili-Q water at the ratio of 1:0.5:0.5 with stirring for 5 seconds by vortex (Ananlog Vortex Mixer). This kind of sol-gel is gelled very fast about 6 minutes.

After the sol-gel solution preparation has been done, we can begin to coat the sol-gel on the fiber surface. The fiber should be without plastic protection jacket in the coating process and cleaned very well. There are many methods which can be used to

clean the fiber. For instance, the mixture of H_2O_2 and H_2SO_4 and the mixture of H_2O_2 ,

$NH_3 \bullet H_2O$ and H_2O are good chemicals to clean the oil and dust on top of the fiber.

NaOH is another good chemical to do this. NaOH can slightly etch a layer of the fiber

depending on the concentration of the NaOH and then the oil and dust on top of the

fiber will also be taken off in this procedure. In addition, ethanol and acetone are

common cleaning chemicals in the semiconductor engineering. In our work, the

fiber is immersed into the 0.1M NaOH solution for 2 hours and then washed by

ethanol for four times. In the coating process, the dipping method is usually used. The

fiber should be very straight and vertical and inserted and pulled out from the sol-gel

solution at a same speed. This can be controlled by a computer controller. Although

the sol-gel film has plenty of pores and the thickness is not the same in the whole film,

the average thickness of the film is proportional to the dipping speed which means the

faster the speed, the thicker the film. In our work, we used the speed of 0.2mm/s. In

our experiment, we usually coat the fiber from the distal end to the LPG (without LPG)

with sol-gel, about 4cm long. The sol-gel film can be dried and hardened in the room

temperature and it also can be hardened and dried in an oven to accelerate the process.

The temperature can't be too high as the PEG which is a composition of the sol-gel

film is an organic chemical. The temperature is usually set at 60 centigrades or 70

centigrades in our work if we want to dry our sol-gel film in the oven.

This kind of sol-gel is a medium pore sol-gel film with the pore size at about

10nm. There is no method to measure the refractive index and thickness of the film on the fiber. We can coat the film on the silica slide with a layer of SiO_2 on top of it and then use ellipsometer to test the thickness and refractive index. The surface of the sol-gel film (Figure 3.4) is very rough and the ellipsometer require a very smooth surface, so not every point of the surface works for ellipsometer. In my experiment, we coated 10 slides with sol-gel film and found 5 points on each film which worked for the ellipsometer and made the average of the refractive index and thickness with the 50 values and we only can get an approximate value. The average thickness for this kind of the sol-gel is about 210nm and the refractive index is about 1.3400, which is low due to open pore structure.
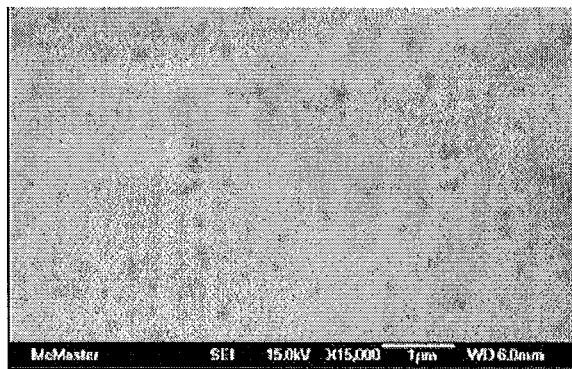

Figure 3.4 The SEM image of this kind of sol-gel film

2.2 Gold nano-particles preparation

Based on the test above, the refractive index of the sol-gel derived silica film is too small, far from the optimal RI in the simulation results. The gold nano-particle is brought in our experiment which is added into the sol-gel film to enhance the

refractive index.

Gold nano-particles are suspension of sub-micrometre-sized particles of gold in a fluid. The liquid is usually either an intense red colour o r a dirty yellowish colour. Modern scientific evaluation of gold nano-particles began from Michael Faraday's work of the 1850s. It has a variety of applications in electronics, nano-technology, chemical and biochemical engineering.

The gold nano-particle solution is made by gold chloride (Gold (III) chloride trihydrate 99.9+% metal basis) and sodium citrate. When the gold chloride is dissolved in the water, it will generate the Au^+. The sodium citrate works as a reducing agent which can donate an electron to the Au^+ and change it to the Au particles. In our experiment, we used 7.89 mg gold chloride dissolved in 20mL Mili-Q water. The solution was heated with stirring on a hotplate until it boiled followed by addition of 2mL of 1.14% sodium citrate solution. The color of the solution changed to the purple showing the presence of gold nano-particles. The gold nano-particles fabricated by this process are usually about 5nm in diameter. After the fabrication process, the gold nano-particle solution should be cooled for more than 3 hours. The wavelength absorbance should be checked by TECAN multifunction micro-plate reader.. If the peak of the wavelength absorbance is around 525 nm, the gold nano-particle solution is fabricated successfully [34].

The sol-gel film with gold nano-particles is usually mixed by sol-gel precursor, mixture of 20% PEG and 200mM HEPES, gold nano-particle solution at the ratio of 1:0.5:0.5 and also coated on the fiber at the speed of 0.2mm/s. In my experiment, we also coated 10 slides with sol-gel film and found 5 points on each film which worked for the ellipsometer and made the average of the refractive index and thickness with the 50 values as in the un-doped sol-gel refractive index measurement and we only can get an approximate value. The refractive index of this kind of sol-gel film is from 1.4-1.45 and the average of the fifty refractive indices is about 1.432 which is also far from the sensitivity enhancement requirements. The initial gold nano-particles which are entrapped in the sol-gel film coated on the fiber can be grown to a larger size. In the gold nano-particle grown work, the fiber with sol-gel film including gold nano-particles is incubated in the 10mM gold chloride solution for 1 hour firstly and then it is immersed into the 0.1M Sodium Borohydride or 1.14% sodium citrate which works as a reduce agent. There is no method to measure the size of the gold nano-particles which are in the sol-gel film on the fiber. However, according the previous work, the gold nano-particles can be grown to 20-30nm in the solution assay [34]. The refractive index of the grown gold nano-particles doped sol-gel film can only also be measured as the ungrown gold nano-particles doped sol-gel film and undoped sol-gel film. The 50 values of refractive indices is from 1.55-1.65 and the average value is about 1.574 which is also not in the sensitivity enhancement

requirement which should be more than 1.75 but it is close and we can observe some

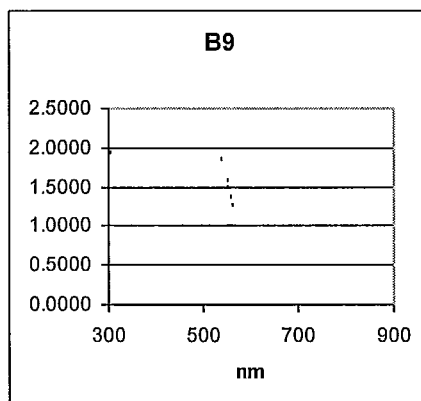sensitivity enhancement by using this kind of film for biosensing [33].

Fig ure 3.5 Gold nano-particle absorbance spectrum

3 Experimental

There are several objectives in this experiment: firstly, the aptamer

immobilization should be demonstrated successfully on the fiber; secondly, the target

should be demonstrated successfully to bind with the aptamer; thirdly, the

performance of the bare fiber device, the sol-gel without gold nano-particles device

and sol-gel with grown gold nano-particles device should be compared to demonstrate

the sensitivity enhancement by adding the sol-gel film and gold nano-particles;

fourthly, selectivity of the aptamer immobilized on the fiber should be demonstrated

and the responses of the results to different target molecule concentrations should be
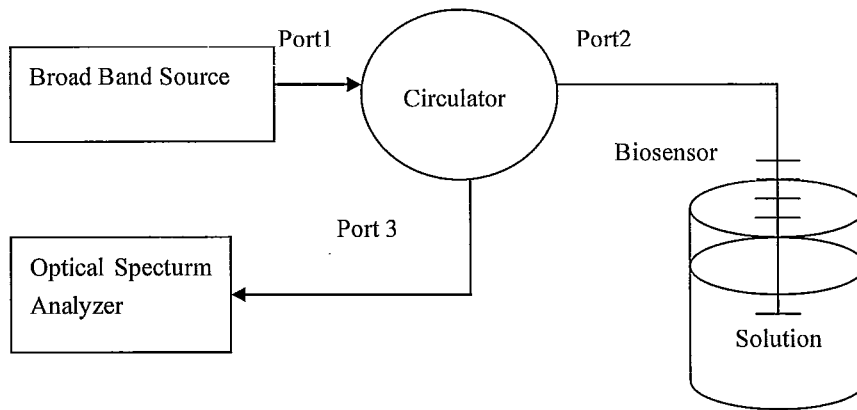
researched finally.

Figure 3.6 Experiment Setup

In the whole process, the fiber was fixed on a computer controller and immersed into the solution controlled by the controller (New Port Universal Motion Controller Driver Model ESP 300 and New Port Motion Controller Model MM3000). Each time, the fiber was immersed into the solution for the same length and we should ensure the long period grating is always exposed to the air and only the sol-gel film coating part is immersed into the solution. The long period grating in the sensor we used with central wavelength between 1560-1570nm. Its bandwidth is about 20-30nm and the notch depth is about 5dB. The grating is about the 2.5cm long and the extra part of the sensor is about 4cm long which is coated by the sol-gel. The experiment setup is as Figure 3.6.

Circulator is an optical component with 3 ports. When the light is incident into port 1, it will go out from port 2 and won't go out from port 3. When the light is

incident into port 2, it will go out from port 3 and won't go out from port1. In our experiment, a broadband source (fabricated by JDS Uniphase Corporation) is used as the light source. The light comes out from the light source and is incident in port one of the circulator. It will go out from port 2 and be injected into the optical fiber biosensor. When the light meets the gold mirror at the distal end, it will be reflected by the gold mirror and incident to port 2 of the circulator again. After that, the light with biosensing signal will go out from port 3 to the optical spectrum analyzer and be recorded by it. As the spectrum of broadband source is not flat with the same power in every wavelength, the calibration should be done first. Then the spectrum of the light which passes the circulator and biosensor is also recorded. Use the latter spectrum to minus the original one and we can get the spectrum of the biosensor. As the current optical spectrum analyzer in our lab only can detect 1000 sample points in the spectrum, the test spectrum range is set to 10nm which is from 1560nm- 1570nm, so the resolution is 0.01nm.

Standard oligonucleotides were prepared by automated DNA synthesis using cyanoethylphosphoramidite chemistry (Keck Biotechnology Resource Laboratory, Yale University; Central Facility, McMaster University), and purified by reversed-phase HPLC as described elsewhere. Adenosine triphosphate (ATP) were obtained from Sigma (Oakville, ON). Sodium silicate (SS, technical grade, 9% Na_2O, 29% silica, 62% water) and aminopropyltriethoxysilane (APTES) were

purchased from Fisher Scientific (Pittsburgh, PA). Water was purified with a Milli-Q

Synthesis A10 water purification system [32].

The target molecule we used in this experiment is Adenosine triphosphate

(ATP) which is a multifunctional nucleotide used in cells as a coenzyme. ATP

transports chemical energy within cells for metabolism. In this work, the refractive

index of sol-gel derived silica film without grown gold nano-particles is about 1.3400

and the refractive index of sol-gel derived silica film with gold nano-particles is about

1.5500. In every experiment, we use three kinds of fiber sensor, the bare fiber device,

the sol-gel with gold nano-particle device and sol-gel with gold nano-particle device.

On the surface of the sol-gel film, it has the –OH. It needs to be changed by

–NH$_2$ in order to immobilize the biomolecules. In our experiment, we used 99%

3-aminopopropyltrethysy silane (APTES) and glacial acetic acid to do this. We mixed

400uL glacial acetic acid, 400uL APTES and 10mL Mili-Q water together and

incubate our fiber sensors in it for 10hours with stirring. After that the biotin can be

attached on top of –NH$_2$. EDC and DSC can also be mixed with biotin in order to

accelerate the diffuse of biotin and the process. In our experiment, we used 150mg

DSC, 60mg EDC and 6mg biotin dissolved in 10mL MES buffer and incubated our

fibers in this solution for 12 hours with stirring. Before this step, we needed to use

MES buffer to wash the fibers for four times. With high affinity to biotin, the

streptavidin molecules can attach to the fiber surface through one of their four binding sites to biotin while leaving others available for further reaction. In our experiment, the fibers should be washed by the 1 x PBS buffer for four times firstly and then incubated in the 500uM streptavin dissolved in 1 x PBS buffer solution for 12 hours. The last step for the immobilization is ATP aptamer immobilization. The ATP aptamer is a kind of DNA whose structure is shown in Figure 3.7 with a biotin linked on one end and a fluorescence molecule. Washed the fiber with 1 x ATP aptamer buffer and then incubated in the 100nM ATP aptamer in 1 x ATP buffer solution for 12 hours.

In the biotin, streptavidin and ATP aptamer immobilization step, the spectrum was recorded every 15 minutes in the first 6 hours and every 30 minutes in the following 4 hours. In order to demonstrate our biomolecules binding are not non-specific binding, a control experiment was also done. Several fiber sensors were divided into two groups. One group of fiber sensors went through biotin immobilization step and the other group of fiber sensors didn't go through the biotin immobilization step. Then both of them went through the streptavidin immobilization step and the spectrum for both groups of fiber sensors were recorded and compared.

$^{5'}$Biotin-TTTTTTTTTTTCACTGACCTGGGGGAGTATTGCGGAGGAAGGT

Figure 3.7 Structure of the ATP aptamer

ATP was used as the target biomolecules in our experiment. We also used another type of biomolecule which was called QDNA. QDNA is a kind of DNA with 12 deoxyribonucleic acids and a fluorescence quench molecule (Figure 3.8). QDNA is fabricated by Yingfu Li's lab in Mcmaster University and used to quench the fluorescence in the fluorescent biosensor when it is binding with ATP aptamer. When the fiber sensor immobilized with ATP aptamer and QDNA was immersed into the ATP solution. The ATP can bind with the ATP aptamer and kick off the QDNA (Figure 3.9). In our work, we did two experiments. The first one was first binding QDNA on the ATP aptamer and then binding ATP on the ATP aptamer with kicking off the QDNA. As the QDNA is not a necessary step in the ATP detection of label-free biosensor, we also did a direct binding of ATP without the QDNA step. In the QDNA and ATP detection work, the concentration of QDNA is 300nM and the concentration of ATP is 1mM. Both work should be done in the 1 x ATP buffer and the fiber sensors also should be washed four times in 1 x ATP buffer before the experiment. In both experiments, bare fiber device, sol-gel device without gold nano-particles and sol-gel device with gold nano-particles were used. In the detection work, we measured the spectrum every 1 minute in the first ten minutes and every two minutes in the following ten minutes and every 10 minutes in the last 100 minutes. The results of the two experiments were recorded and compared.

GTGACTGGACCC$_5$'

|

Q

Figure 3.8 Structure of ATP QDNA

The selectivity work has also been done which includes two groups of work,

using ATP aptamer to detect wrong target and use wrong aptamer to detect ATP. In our

first experiment, we used ATP aptamer to detect thrombin QDNA (Figure 3.10),

Guanosine triphosphate (GTP), Uridine 5'-triphosphate (UTP) and Cytidine

triphosphate (CTP). The concentration of the thrombin QDNA solution is the same

with the ATP QDNA solution in the previous experiment and the concentration of the

GTP, UTP and CTP solution is the same with ATP solution in the previous experiment.

In our second experiment, we used the thrombin aptamer (Figure 3.11) to detect the

ATP. The immobilized thrombin aptamer is the same with the ATP aptamer in the

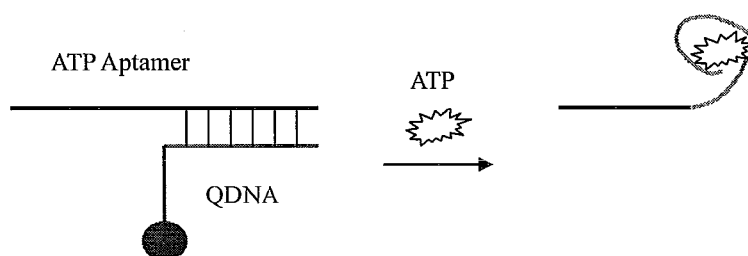previous work and the immobilization steps are the same.

Figure 3.9 QDNA and ATP binding

GTGACACCAACC$_5$'

|

Q

Figure 3.10 Structure of Thrombin QDNA

^{5'}Biotin-TTTTTTTTTTTCACTGTGGTTGGTGTGGTTGG

Figure 3.11 Structure of Thrombin Aptamer

At last, we tried different concentrations of the ATP solution from 0 -2.5mM.

We tried 250uM, 500uM, 750uM, 1mM, 1.5mM, 2mM and 2.5mM

Those discussed above are all the details of the experiments. The results of the

experiments will be discussed in the Chapter 4.

Chapter 4 Results and discussion

When the LPG is spliced with the biosensor cavity with the gold mirror at the distal end, we can view several clear interference fringes in the spectrum of the biosensor (Figure 4.1) and can use this biosensor for biosensing detection. In this chapter, we present experimental fiber biosensor responses to the biosensing experiments described in Chapter 3. As presented in chapter 3, three groups of fiber sensors were used, bare fiber devices, devices with sol-gel without gold nano-particle and devices with sol-gel and gold nano-particles. In each group, there are four fiber optical biosensors. Although all the sensors are fabricated in the same procedure, there are some small differences between the four fibers in gold mirror fabrication, LPG fabrication, splicing and sol-gel film coating. In addition, there is also some background noise which is a random signal added in the main biosensing signal, so there can be some differences in the signal of the four biosensors in the same group. The figure presenting the relation between wavelength shift and time is the average of the four fibers and the figure presenting the optical spectra before a nd after the binding process is selected to be representative of biosensors in this group.
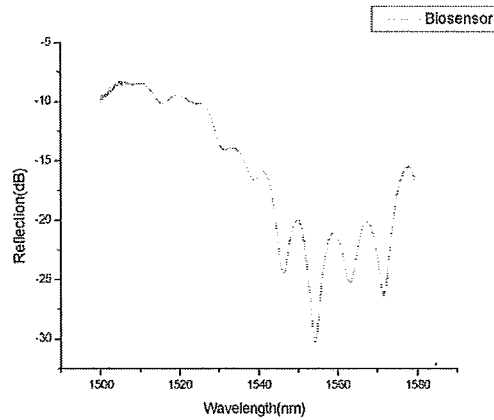
Figure 4.1 The spectrum of one biosensor

Three types of fibers were prepared as described in Chapter 3. The first was a bare fiber device. The second is a device with a porous sol-gel film and the third is a device with a grown gold nano-particles doped sol-gel. Figure 4.2 shows the result of the wavelength shifts upon biotinylation of the three fiber surfaces. Figure 4.3 shows the wavelength shifts upon addition of streptavindin and Figure 4.4 shows the wavelength shift upon addition of ATP aptamer.
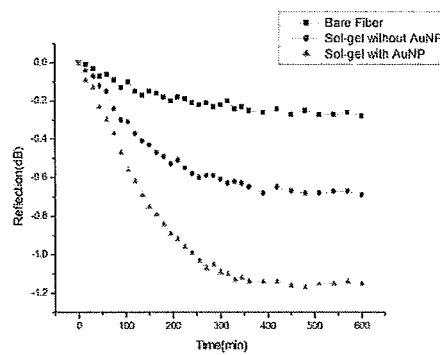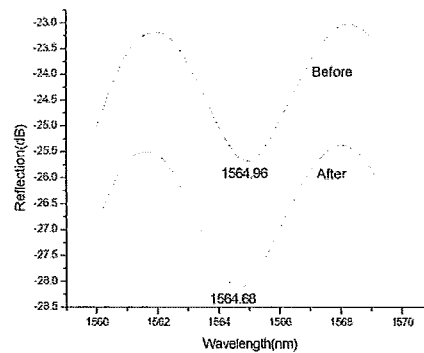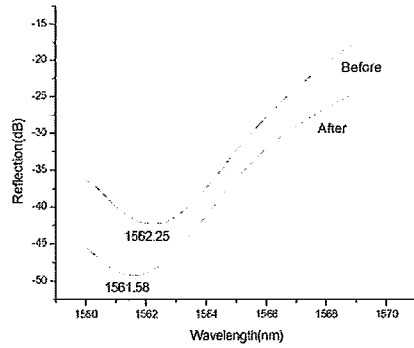

(a)

(b)
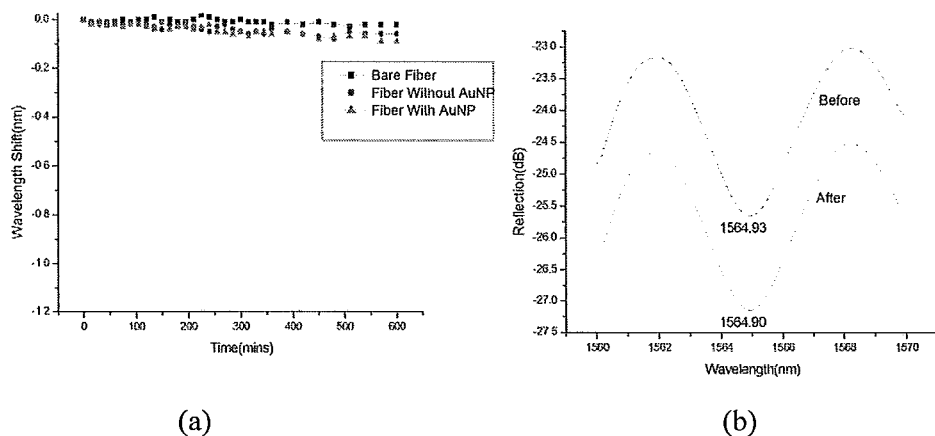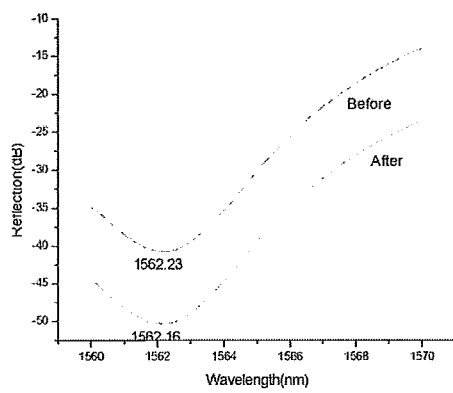
(c)
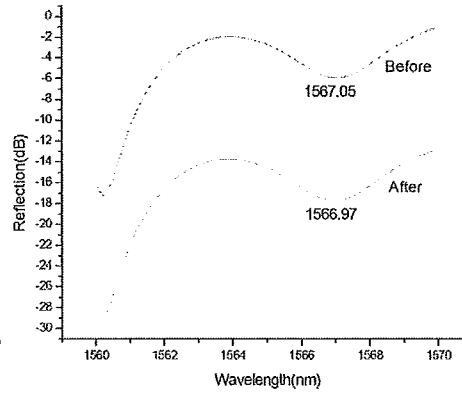
(d)

Figure 4.2 The result of biotin binding. (a) The relationship of the average of the four biosensors in

each group and time; (b)One device in the bare fiber group; (c)One device in the sol-gel without

gold nano particle group; (d) One device in the sol-gel with gold nano-particle group
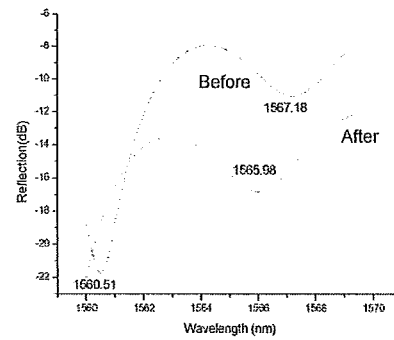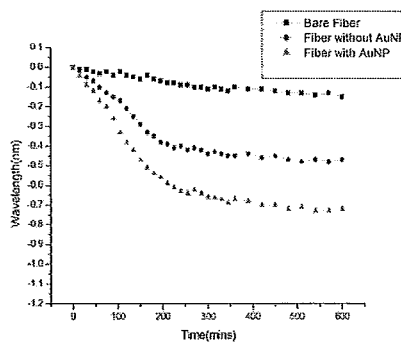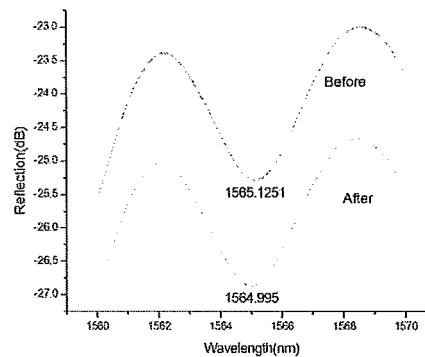

(a)

(b)

(c)

(d)

Figure 4.3 The result of streptavidin binding. (a) The relationship of the average of the four

biosensors in each group and time; (b)One device in the bare fiber group; (c)One device in the

sol-gel without gold nano particle group; (d) One device in the sol-gel with gold nano-particle

group

(a)

(b)

(c)   (d)

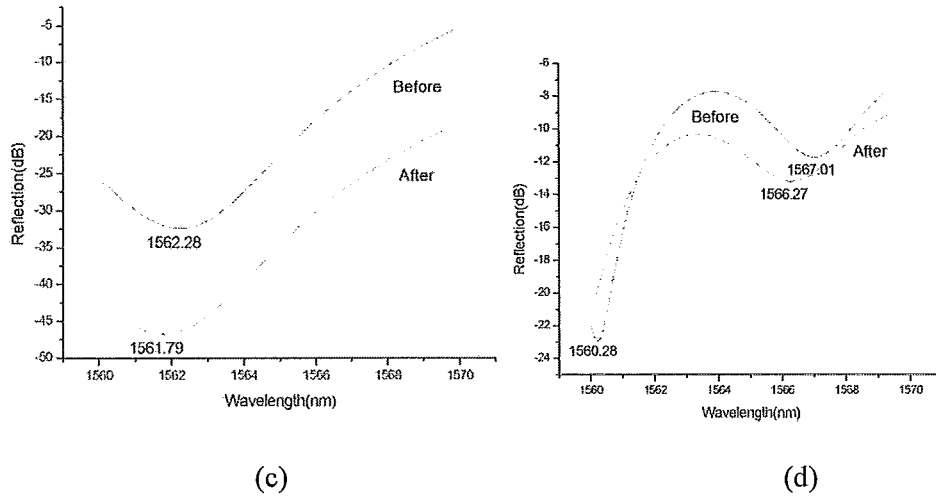Figure 4.4 The result of ATP aptamer binding. (a) The relationship of the average of the four

biosensors in each group and time; (b)One device in the bare fiber group; (c)One device in the .

sol-gel without gold nano particle group; (d) One device in the sol-gel with gold nano-particle

group

There are wavelength shifts in all three groups of the devices in all the three

steps which means that there are biomolecules binding on the fiber and all the three

kinds of sensors work for biomolecule immobilization. All the wavelengths move to

shorter wavelengths as the refractive index of the solution around the fiber sensor is

increased upon binding of biomolecules on the fiber surface. In comparing the

wavelength shifts between devices, the bare fiber shows the smallest followed by the

undoped sol-gel film device (2-3 folds enhancement) and the gold nano-particles

doped sol-gel film device (1.5-2 folds enhancement than the undoped film). The

sol-gel with gold nano-particles experiences the largest wavelength shift as the

refractive index and thickness of the overlay approaches the sensitivity enhancement

requirements outlined in Chapter 2 although it doesn't exactly fit the requirements.

Also the undoped sol-gel coated device experiences a larger wavelength shift than the

bare fiber device as the surface of the sol-gel film is very rough and has a much larger

surface than the bare fiber, and a larger binding density. In order to better observe the

whole process of the immobilization experiments, we measured the spectrum every 15

minutes in the first 6 hours and every 30 minutes over the next 4 hours. The results of

the wavelength and time relationship are the average of the four fibers. We can see the

wavelength moves faster in first a few hours and becomes slower in last a few hours

and it approaches a fixed value at last which means the binding is nearly finished (see

Figure 4.2 (a), Figure 4.3 (a) and Figure 4.4 (a)). We can clearly see the wavelength

shifts of the biotin (Figure 4.2) are much smaller than the streptavidin (Figure 4.3).

The wavelength shifts of the ATP aptamer (Figure 4.4) are also smaller than

streptavidin but larger than biotin. In these three types of molecules, streptavidin is a

relative large biomolecule whose molecular weight is about 53 kDa and can contribute

a large refractive index change around the fiber when it is binding on the fiber. The

ATP binding aptamer, whose molecular weight is about 21 kDa, is a smaller

biomoleculethan streptavindin but larger than biotin, whose molecular weight is 244

Da. However, the relationship between the wavelength shift and the molecule weight

is not linear because the concentration influences the signal and the difference in the

intrinsic structure of different biomolecules may alter the signal.

Given the significant wavelength shifts in the immobilization step, it was clear

that the ATP aptamer was successfully immobilized on the device. As a Next step, the

sensor was used to detect a QDNA strand whose molecular weight is about 3700 Da,

which binds the ATP aptamer via hybridization.. The bio-detection step (Figure 4.5)

was much faster than the aptamer immobilization step, occurring in 1- 2hours. In our

experiment, we measured the spectrum every 1 minute in the first 10 minutes, every 2

minutes in the next 10 minutes and every 10 minutes in the last 100 minutes. As

shown in Figure 4.5, the wavelength shifts to shorter wavelength as the QDNA binds

to the device and enlarges the concentration of the solution around the fiber. Figure

4.6 is the result of ATP detection after the QDNA hybridization step. In the case of

ATP detection after QDNA immobilization, the wavelength moves to a longer

wavelength. In this step, binding of two ATP molecules to the ATP aptamer and

removes one QDNA. Compared to the initial concentration around the fiber sensor,

the refractive index decreased as the ATP molecule replaced the QDNA molecules.

Also, we can see the difference between the grown gold nano-particles doped sol-gel

device, undoped sol-gel device and bare fiber device are as expected as the earlier

immobilization experiments. The wavelength shift of the grown gold nano-particles

doped sol-gel device is also about 1.5-2 times of the ones of the sol-gel without gold

nano-particle device. The wavelength shifts of the undoped sol-gel device is also

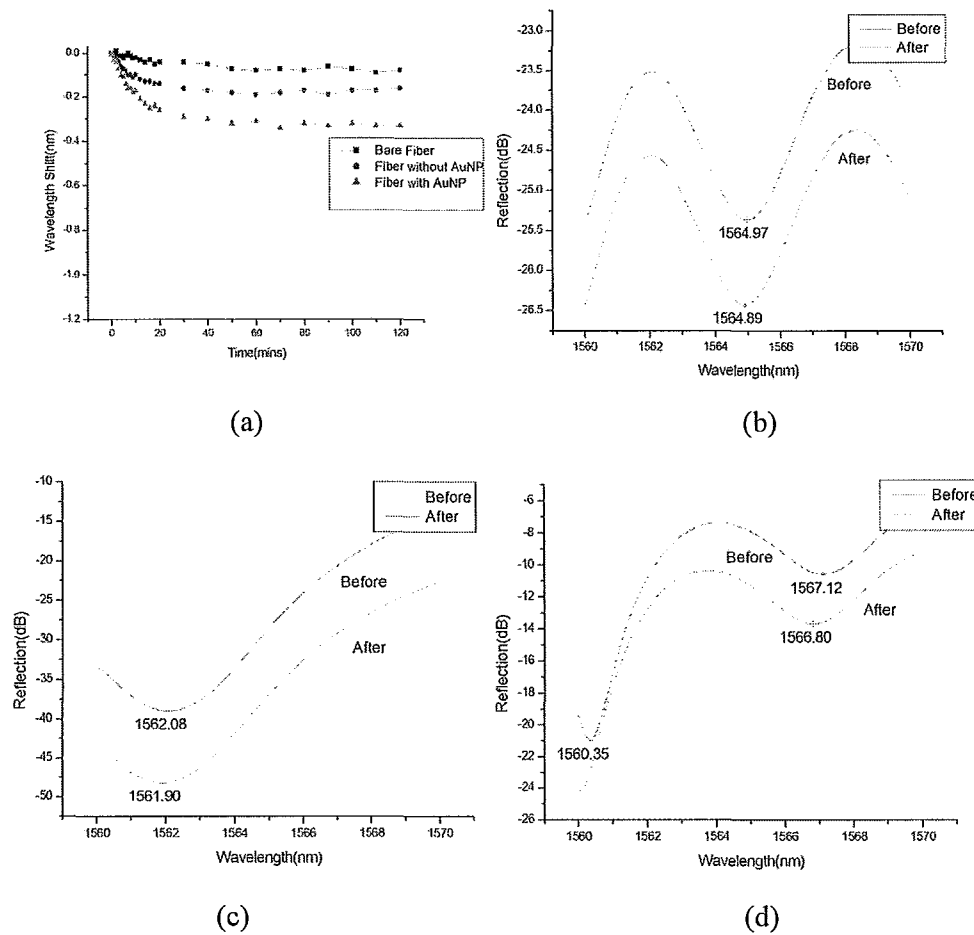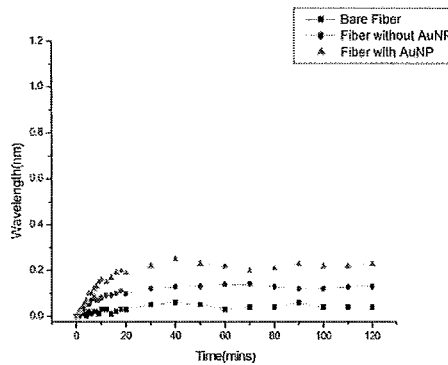about 2-3 times of the bare fiber device.

(a)

(b)

(c)

(d)

Figure 4.5 The result of ATP QDNA detection. (a) The relationship of the average of the four

biosensors in each group and time; (b)One device in the bare fiber group; (c)One device in the

sol-gel without gold nano particle group; (d) One device in the sol-gel with gold nano-particle

group

In the case of ATP detection with bind QDNA, the sensor binds two ATP

whose molecular weight is 501 g/mole and loses one QDNA strand whose molecular

weight is about 3300 g/mole for a molecular weight loss of about 2300 g/mole. This is

accompanied by a large change in ATP apatmer structure which is likely to influence

the refractive index change and wavelength shift. The QDNA is not a necessary step in a label-free biosensor detection but does have an "inverted" signal change which can improve the sensitivity. The ATP detection was also done without QDNA to produce a full label-free biosensor (Figure 4.7). From the results, we can see the wavelength now moves to shorter wavelengths as the ATP is just binding with ATP aptamer and not removing a QDNA into the solution as in the previous experiment. However, the signal change is smaller as the molecular weight change is smaller which suggests that very large QDNA may provide a way to increase sensitivity. Once again, we also can see the difference in the wavelength shifts among the three groups of devices.

(a)   (b)

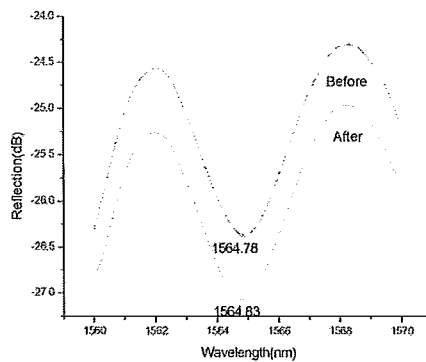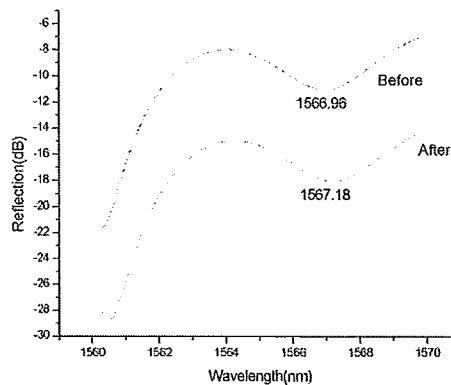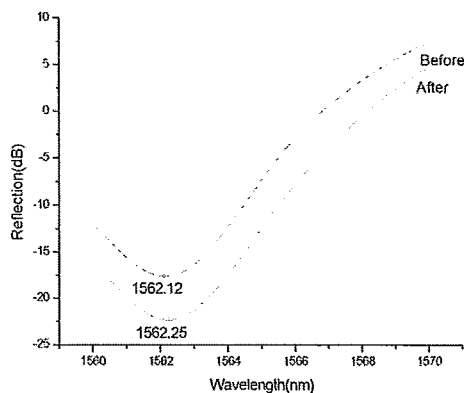(c)   (d)

Figure 4.6 The result of ATP detection after ATP QDNA step. (a) The relationship of the average of

the four biosensors in each group and time; (b)One device in the bare fiber; (c)One device in the

sol-gel without gold nano particle; (d) One device in the sol-gel with gold nano-particle

(a)   (b)

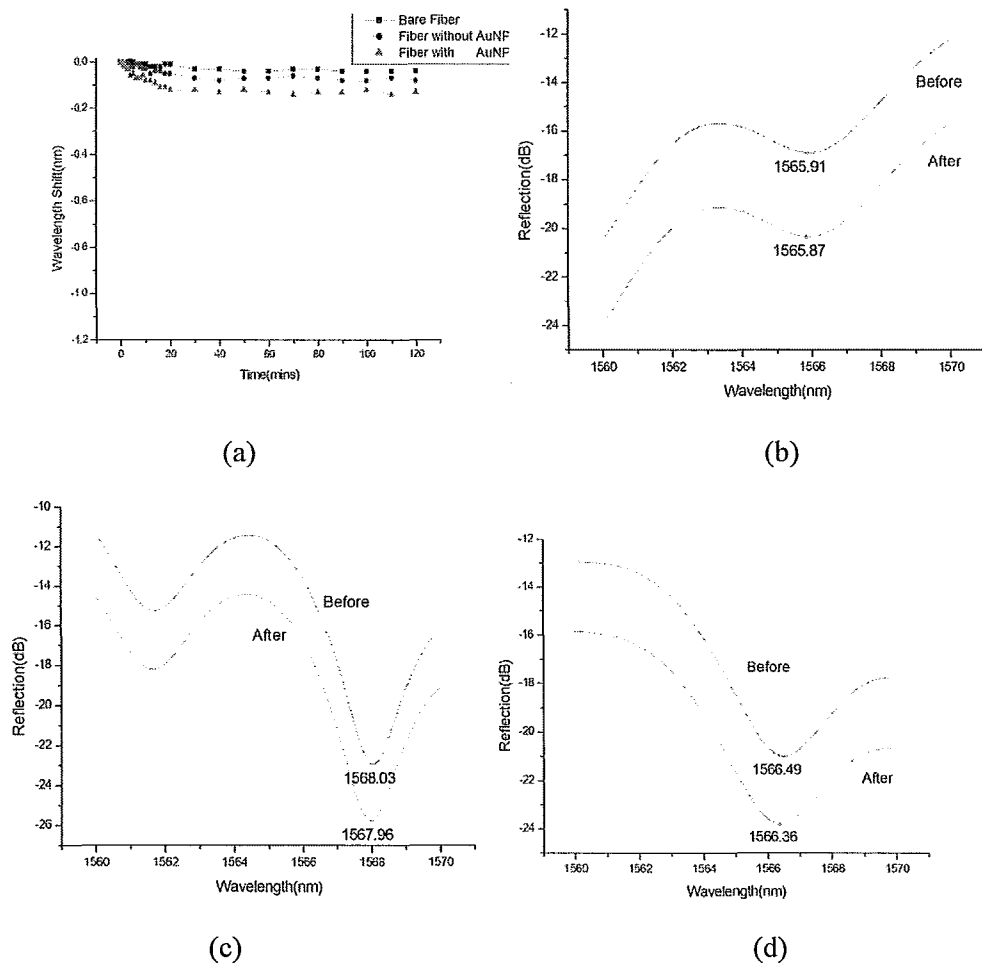(c)   (d)

Figure 4.7 The result of ATP detection without the ATP QDNA step. (a) The relationship of the

average of the four biosensors in each group and time; (b)One device in the bare fiber group;

(c)One device in the sol-gel without gold nano particle group; (d) One device in the sol-gel with

gold nano-particle group

Table 4.1 is a conclusion of the results for the aptamer immobilization and bio-molecule detection. The results are the average of the four devices in each type of biosensor. The negative value means the wavelength moves to the shorter wavelength and positive value means the wavelength moves to the longer wavelength. It shows the multiple steps of enhancement can produce about 6 folds better signal and higher sensitivity (inverted signal). The value is the bracket is the standard deviation of the four fibers in each group and experiment.

Wavelength Shift (nm)	Biotin	Streptavidin	Aptamer	QDNA	ATP (After QDNA)	ATP (directly)
Bare fiber	-0.02 (0.01)	-0.28 (0.04)	-0.15 (0.01)	-0.08 (0.03)	0.04 (0.01)	-0.04 (0.02)
Normal Solgel	-0.06 (0.01)	-0.69 (0.03)	-0.47 (0.06)	-0.16 (0.02)	0.13 (0.02)	-0.08 (0.03)
Sol-gel with AuNP	-0.09 (0.02)	-1.15 (0.07)	-0.72 (0.04)	-0.33 (0.04)	0.23 (0.02)	-0.13 (0.02)

Table 4.1 Results of ATP aptamer immobilization and bio-molecule detection with 1mM ATP

In order to demonstrate the results above are not non-specific binding, we also

did a control experiment to detect the signal from potential interferents. We used two groups of devices. One group went through the biotin binding step and the other group didn't go through the biotin binding step. Both of the two groups used the fiber with sol-gel and gold nano-particles. Then both groups are measured in the streptavidin solution. The results are shown in Figure 4.8. The measurement continues for 3 hours and we can see there is an obvious signal in the sensor groups that went through the biotin immobilization and there is only a weak signal fluctuated near zero in the sensor groups that didn't go through the biotin immobilization. The signal of the devices that went through our immobilization steps is much larger than the non-specific binding signal. This successfully demonstrated that our immobilization steps are selected and are not based on non-specific binding.

(a)   (b)
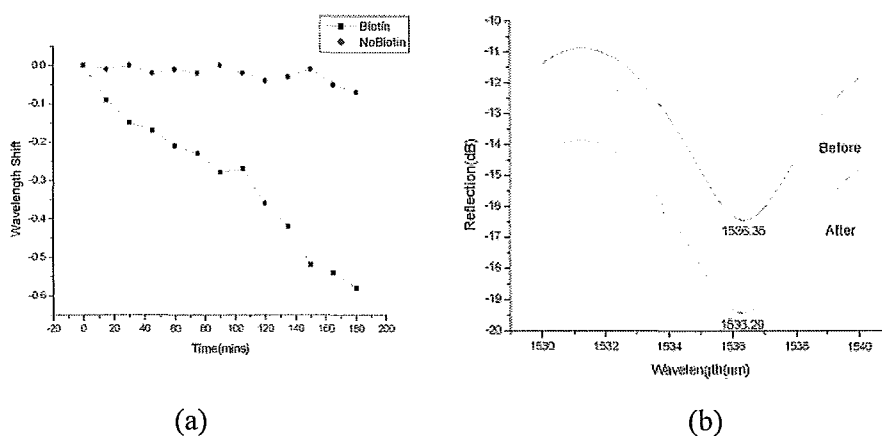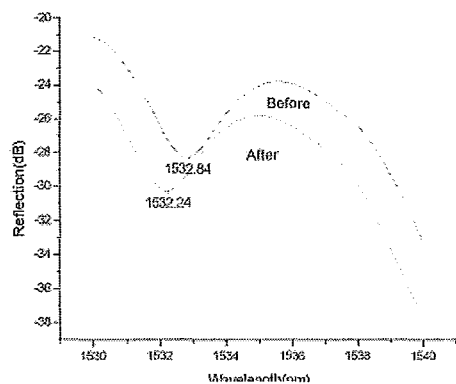
(c)

Figure 4.8 (a) Signal comparison of the devices without biotin step and with biotin step (b) The

spectrum of the devices without biotin step (c) The spectrum of the devices with biotin step

Selectivity work is also an important goal in our research. In order to

demonstrate the selectivity of the aptamer also works on our fiber sensor, we first used

the ATP aptamer to detect the potential interferents, QDNA for a thrombin

structure-switching aptamer, CTP, UTP, GTP. We used a thrombin aptamer to detect

ATP. The concentration of the thrombin QDNA is the same with the ATP QDNA in the

previous step which is 300nM. The concentration of the CTP, UTP, GTP are the same

with ATP in the previous steps which is 1mM. The measurement time is also 2 hours

as in the previous steps. In all of the five experiments, the fiber sensor utilized the

gold nano-particle doped sol-gel device. The results are shown in Figure 4.9. All the

five figures are compared the results of this kind of experiments (right aptamer and

wrong target or right target and wrong aptamer) with the previous experiments (right

target and right aptamers). We can clearly see that there is nearly no signal (only some

minor non-specific binding and background noise signal) when we used wrong

aptamer or wrong target. However, there is an obvious signal, when we used both the

right aptamer and the right target. This demonstrate the selectivity of the aptamer also

works well when the aptamers are binding on the fiber sensor.

In order to further research the ATP detection by the aptamer, we measured the

signal as a spectrum of ATP concentration over the range of 0- 2.5mM, using the fiber

sensor with the gold nano-particles doped sol-gel films. Figure 4.10 shows the average

of the four fibers in each concentration. From Figure 4.10, the signal is enhanced very

rapidly in the first few concentrations. When the concentration is larger than 1mM, the

singal increase more slowly
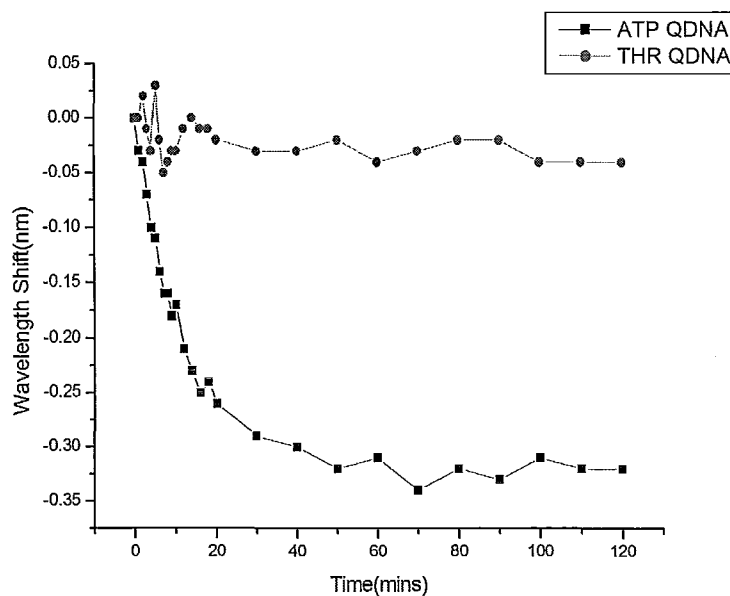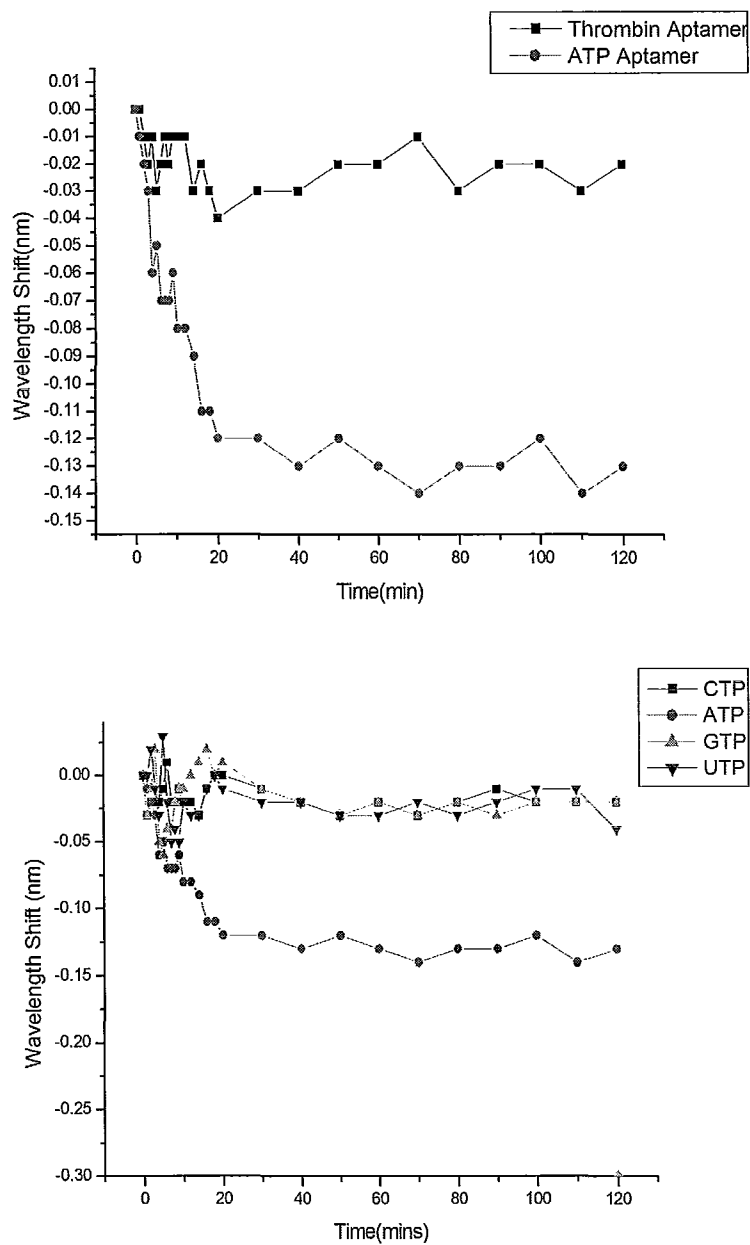
Figure 4.9 (a)Detection of ATP aptamer to thrombin QDNA (b) Detection of thrombin aptamer to

ATP   (c) Detection of ATP aptamer to GTP
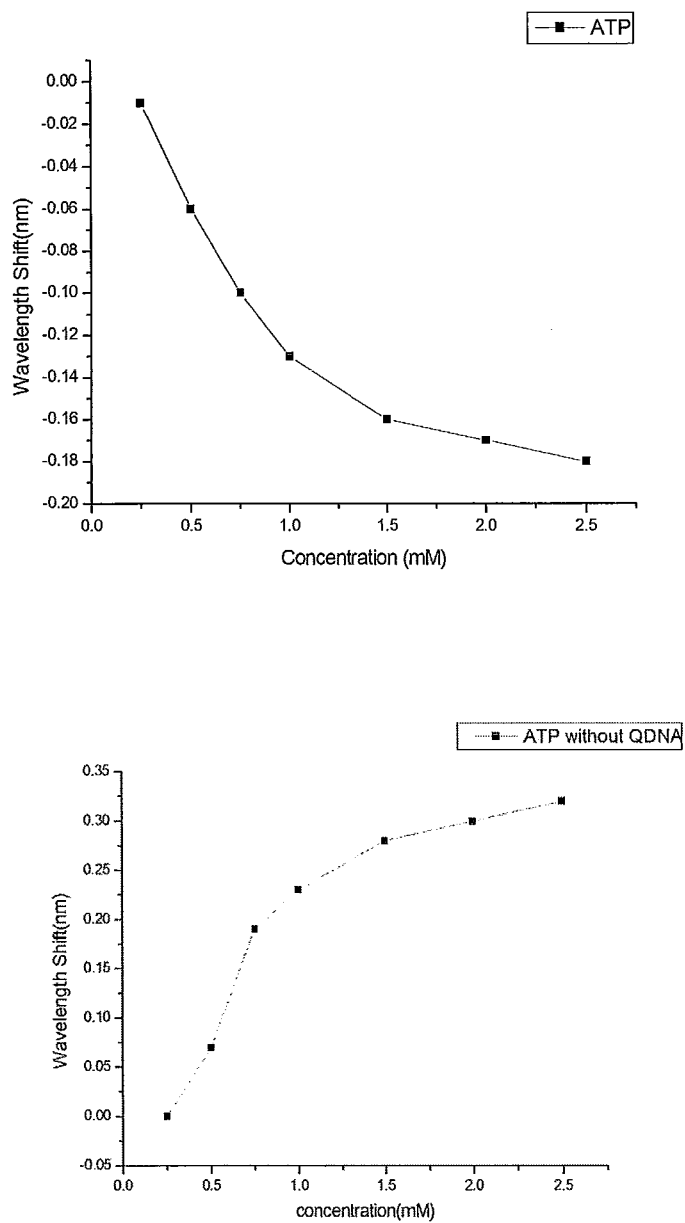
Figure 4.10 Relationship between wavelength shift and concentration a) ATP without QDNA step

b) ATP with QDNA step

The experimental data presented in this chapter shows the biosensor can work

for the biosensing detection and it has good selectivity. The sol-gel film with gold

nano-particles also works well for the sensitivity enhancement.

Chapter 5 Summary and Future Work

1 Summary and conclusion

It is the first time to combine a bio-compatible film with other LPG biosensor platform and implement the biosensing detection with good selectivity. The device used was an in-fiber Michelson interferometer structure. It was made by a piece of fiber with a long period grating inscribed in it and a gold mirror at the distal end. Then a layer of film was coated on top of the fiber head. The film can cause the mode reorganization phenomenon and enhance the sensitivity if it has a suitable refractive index and thickness. If the refractive index is larger, the thickness is needs to be smaller. As we wanted more evanescent wave penetrating into the ambient, the thickness is usually set to be small and refractive index is set to be large. In our work, the thickness is set to be 210-250nm and the target refractive index is about 1.75.

Much previous work about the film has been done and reported before. However, some film deposition methods are not suitable for the fiber which is a very thin and cylindrical structure, such as most of film growth and deposition technique in the semiconductor engineering. Other film deposition methods are suitable for the fiber. For instance, in the previous work in this topic, a polymeric nano-film (PAA/PAH) with silver particles is used in the sensitivity enhancement work, but it is not easy to make this film to be bio-compatible and immobilize bio-molecules such as aptamers. Sol-gel derived silica films are both easy to deposite on the fiber and

amenable to bimolecule immobilization. This film is used in our work to be immobilized with aptamer and detect the ATP solution. We also added gold nano-particles to enhance the refractive index of the sol-gel derived silica film.

Three types of devices were fabricated in our work. One was bare fiber device. One was the device coated by the standard sol-gel film. The other was the device coated by the sol-gel film with gold nano-particles. The performance of the three types of devices was measured in our work. The signal of the device coated by the standard sol-gel film was much larger, about 3 times, than the bare fiber device, because the surface of the sol-gel derived silica film was porous which made the surface area of the sol-gel film was much larger than the bare fiber. Then there were much more bio-molecules binding on the sol-gel film surface than the bare fiber surface. We also could see some differences between the device coated by the standard sol-gel film and the device coated by the sol-gel film with gold nano-particles. The signal of the sol-gel with gold nano-particle device is about 1.5-2 times than the standard sol-gel device. Although the refractive index of the sol-gel film is not easy to be enhanced, the gold nano-particles still work to some extent to enhance the sensitivity.

It also can be seen from the results that the signal is larger if the molecular weight is larger. However, this relationship is not linear due to the difference of the intrinsic structure of different molecules. The concentrations are also a typical

function to influence the signal. We changed the concentrations of the target

biomolecules, ATP and we could see the signal was enhanced when the concentrations

are enhanced.

As there were also some natural adsorbance and non-specific binding in the

biosensing step, the control experiment has also been done. The great difference

between our signal and non-specific binding signal told us the binding in our

biosensing work was not non-specific binding.

Another important work was the selectivity work. The work was divided into

two parts: the first was using right aptamer to detect the wrong target. In this work, we

used the ATP aptamer to detect thrombin QDNA, GTP, CTP and UTP. The second is

to use the wrong aptamer to detect the right target. We used the thrombin aptamer to

detect the ATP. The signals got in these experiments were very small which was very

different from the experiments of right aptamer to detect the right target, which meant

the selectivity of the aptamer also worked in our fiber device.

From the summary above, we can conclude that our biosensor has been

demonstrated to be working for biosensing and have the selectivity. The binding

process is not non-specific binding process. The sol-gel device has larger sensitivity

than the bare fiber device and the gold nano-particles also work for the sensitivity

enhancement.

2 Future work

Although it can show the long period grating based fiber biosensor with sol-gel derived silica film can work for the biosensing, there is still much work need to be done in the future in this project.

The first thing need to be done in the future is to enhance the sensitivity. A previous work with polymeric nano-film (PAA/PAH) with silver particles achieved a much higher sensitivity than the sol-gel film [35]. However, that film is hard to be made to be bio-compatible and then we changed to use the sol-gel film. The refractive index of the sol-gel film is hard to be enhanced which leads that the sensitivity of the sol-gel device can't be enhanced very high. The future work can be done in three areas. Firstly, the method for enhancing the refractive index of the sol-gel film can be researched. For instance, we can continue to grow the gold nano-particles or add other types of chemicals into the sol-gel film such as TiO_2. Secondly, the way to make the polymeric film (PAA/PAH) biocompatible and easy to immobilize the biomolecules can also be researched. Thirdly, another way is to find another film that is both easy to enhance the sensitivity and biocompatible.

Another work need to be done is to change other types of aptamer. The ATP

aptamer immobilization is the simplest one in the biosensing work. The immobilization and fluorescence detection work of ATP on the plane slides has been successfully done before. Our work is only to transfer this technique onto our fiber device. Our aptamers which are not successfully immobilized on the plane slides will be a challenge to implement the biosensing immobilization on fiber.

The third work is to change the biosensing immobilization technique. There is a method called rolling circle amplification (RCA) method. In this technique, a large DNA will be generated and binding on the fiber. As the experiments results shows, the signal is related to the molecular weights. If the concentration of the target DNA is the same with the ATP in this work, the signal is supposed to be much larger in the RCA work.

References

[1] http://en.wikipedia.org/wiki/Sensor, June 10th, 2010.

[2] L. C. Clark, Jr. and C. Lyons, "Electrode systems for continuous monitoring in cardiovascular surgery," *Ann N Y Acad Sci*, 102, pp. 29-45, 1962.

[3] http://en.wikipedia.org/wiki/Biosensor, June 13th, 2010.

[4] D. R. Thevenot, K. Toth, R. A. Durst, and G. S. Wilson, "Electrochemical biosensors: recommended definitions and classification," *Biosensors & Bioelectronics*, 16, pp. 121-131, 2001.

[5] G. P Anderson, L. C. Shriver-Lake, J. P. Golden, F. S. Ligler, "Fiber-optic-based biosensor: signal enhancement in a production model," *Proceedings of SPIE - The International Society for Optical Engineering* 1648, 39-43. 1992.

[6] L. M. Smith, J.Z. Sanders, R.J. Kaiser, P. Hughes, C. Dodd, C.R. Connell, C. Heiner, S.B. Kent, L.E. Hood, "Fluorescence detection in automated DNA sequence analysis," *Nature*, 321, 674-679, 1986.

[7] S. Weiss, "Fluorescence Spectroscopy of Single Biomolecules," *Sc ience*, 283, 1676- 1683, 1999.

[8] Charles T. Campbell, A. Background, "Surface Plasmon Resonance (SPR) Biosensor Development", Citeseer Beta, 2008.

[9] H. Roos, "Biosensor Systems and Biacore Technology," Biacore AB, Upsala, Sweden, 2003.

[10] R. Wolthuis, D. McCrae, E. Saaski, J. Hartl, G. Mitchell, "Development of a

medical fiberoptic ph sensor based on optical absorption," *IEEE Transactions on Biomedical Engineering* 39, 531-537, 1992.

[11] R. A. Wolthuis, D. McCrae, J. C. Hartl, E. Saaski, G. L. Mitchell, K. Garcin, R. Willard, "Development of a medical fiber-optic oxygen sensor based on optical absorption change," *IEEE Transactions on Biomedical Engineering* 39, 185-193, 1992.

[12] X. D. Hoa, A. G. Kirk, M. Tabrizian, "Towards integrated and sensitive surface Plasmon resonance biosensors: A review of recent progress," *Biosensors and Bioelectronics*, 23, 151-160, 2007.

[13] Raman Kashyap, *Fiber Bragg Grating*s, 29-34, 1999.

[14] A.N. Chryssis, S. M. Lee, S. B. Lee, S. S. Saini, M. Dagenais, "High Sensitivity Evanescent Field Fiber Bragg Grating Sensor, " *IEEE Photonics Technology Letters*, 17, 1253-1255, 2005.

[15] H. J. Patrick, A.D. Kersey, F. Bucholtz, "Analysis of the Response of Long Period Fiber Grating to External Index of Refraction, " *J. Lightwave Technology*, 16, 1606-1612, 1998.

[16] C. J. Brinke, G.W. Scherer ; G.W. Scherer, "The Physics and Chemistry of Sol-Gel Processing" *Sol-Gel Science*, 1990.

[17] L. L. Hench, J. K. West "The Sol-Gel Process". *Chemical Reviews* 90: 33, 1990.

[18] A.D. Ellington, J.W.Szostak, "In vitro selection of RNA molecules that bind specific ligands," *Nature* 346 (6287): 818–22, 1990.

[19] L.C. Bock, L.C. Griffin, J.A. Latham, E.H. Vermaas, J.J. Toole, "Selection of single-stranded DNA molecules that bind and inhibit human thrombin". *Nature* 355 (6360): 564–6, 1992.

[20] G. Meltz, W. W. Morey, and W. H. Glenn, "Formation of Bragg Gratings in Optical Fibers by a Transverse Holographic Method," *Optics Letters*, 14, pp. 823-825, 1989.

[21] K. O. Hill, B. Malo, K. A. Vineberg, F. Bilodeau, D. C. Johnson, and I. Skinner, "Efficient Mode Conversion in Telecommunication Fiber Using Externally Written Gratings," *Electronics Letters*, 26, pp. 1270-1272, 1990.

[22] A. Yariv, "Coupled-mode theory for guided-wave optics," Ieee Journal of Quantum Electronics, QE-9, pp. 919-933, 1973.

[23] T. Erdogan, "Cladding-mode resonances in short-and long-period fiber grating filters," 14, 1760-1773, 1997.

[24] T. Erdogan, "Fiber Grating Spectra," *J. Light Tech.*, 15, 1277-1294, 1997.

[25] http://en.wikipedia.org/wiki/Michelson_interferometer, June 26th, 2010

[26] J. Yang, "Long-period Grating Photonic Devices for Biosensing," Doctor of Philosophy, Engineering Physics, McMaster University, 2007

[27] P. Yeh, A. Yariv, and E. Marom, "Theory of Bragg Fiber," Journal of the Optical Society of America, 68, pp. 1196-1201, 1978.

[28] J. Yang, P. Sandhu, W. Liang, C. Q. Xu, Y. Li, "Label- Free Fiber Optic Biosensors With Enhanced Sensitivity," *J. Selected Topics in Quantum Electronics*, 13,

1691-1696, 2007

[29] J. Yang, L. Yang, C. Q. Xu, W. Huang, Y. Li, "Long-period grating refractive index sensor with a modified cladding strucuture for large operational range and high sensitivity," *Applied Optics*, 45, 6142- 6147, 2006

[30] A. Cusano, A. Iadicicco, P. Pilla, L. Contessa, S. Campopiano, A. Cutolo, "Mode transition in high refractive index coated long period gratings," *Optics Express*, 14, 19-34, 2006

[31] R. M. Atkins, P. J. Lemaire, T. Erdogan, and V. Mizrahi, "Mechanisms of Enhanced Uv Photosensitivity Via Hydrogen Loading in Germanosilicate Glasses," *Electronics Letters*, 29, pp. 1234-1235, 1993.

[32] Nicholas Rupcich, Razvan Nutiu, Yingfu Li, John D. Brennan, "Entrapment of Fluorescent Signaling DNA Aptamers in Sol-Gel-Derived Silica," *Analytical Chemistry*, 77:14, 4300-4307, 2005.

[33] B. D. Busbee, S. O. Obare, C. J. Murphy, "An improved synthesis of high-aspect-ratio gold nanorods, " *Advanced Materials*, 15:5, 414-417, 2003

[34] R. E. Luckham, J. D. Brennan, "Bio active paper dipstick sensors for acetylcholinesterase inhibitors based on sol-gel/enzyme/gold nanoparticle composites" *Analyst*, 135:8, 2028-2035, 2010

[35] P. Sandhu, J. Yang, C. Q. Xu, "In-Fiber Michelson Interferometer With Polymeric/Nanoparticle Thin-Film Overlay as a Platform for Biosensing," IEEE Journal of Selected Topics in Quantum Electronics, 16:3, 685-690, 2010.

[36] F. A. Muhammad, G. Stewart, W. Jin, "Sensitivity enhancement of D-fiber methane gas sensor using high-index overlay," *IEEE Proceedings-J*, 140, 115-118, 1993.

[37] I. Del Villar, I. R. Ashwell, R. P. Tatam, "Optimization of sensitivity in Long Period Fiber Gratings with overlay deposition," *Optics Express*, 13, 56-69, 2005.

[38] S. W. James, I. Ishaq, G. J. Ashwell, R. P. Tatam, "Cascaded long-period gratings with nanostructured coatings, " *Optics Letters*, 30, 2197-2199, 2005.